FAST PEAK-POWER REDUCTION FOR MIMO-OFDM SYSTEMS WITH DIVERSITY

BY

THEODOROS TSILIGKARIDIS

THESIS

Submitted in partial fulfillment of the requirements
for the degree of Master of Science in Electrical and Computer Engineering
in the Graduate College of the
University of Illinois at Urbana-Champaign, 2009

Urbana, Illinois

Adviser:

Professor Douglas L. Jones

ABSTRACT

A robust peak-power reduction technique called active constellation extension (ACE) reduces the peak-to-average power ratio (PAPR) of single-input single-output (SISO) orthogonal frequency-division modulated (OFDM) signals by extending the outer constellation points in a way that minimizes the PAPR of an OFDM transmit signal, without reducing the bandwidth or increasing bit error rate (BER).

Recent work includes extensions of the concept of ACE using a modified smart gradient-project algorithm for MIMO-OFDM systems. We extend the efficient ACE smart gradient-project (SGP) method to space-time block coded (STBC), space-frequency block coded (SFBC) and V-BLAST OFDM systems. The proposed peak-power reduction method can be applied to any space-time-frequency (STF) block code, and its performance is bounded by the code structure. Simulations show PAPR reduction gains of 4.19 and 3.57 dB under QPSK for Alamouti STBC and SFBC, respectively.

In addition, we extend the efficient ACE-SGP method to rotated constellations for SISO-OFDM systems, an alternative method recently invented for providing diversity. Simulation results show approximately 3.46 dB and 2.08 dB of PAPR reduction for QPSK and 16-QAM original constellations, respectively, for 256 subcarriers. Results also show that 4.29 dB and 3.41 dB of PAR reduction are obtained for QPSK and 16-QAM original constellations, respectively, for 1024 subcarriers.

Furthermore, we show how the PAPR reduction method known as tone injection can be a very practical transmission scheme for coded-OFDM systems,

with a slight compromise of the BER performance. This is accomplished by developing efficient, near-optimal, convolutional and LDPC decoders for the extended non-bijective constellations introduced by tone injection. Simulation results for convolutional and LDPC coded-OFDM systems show BER performance comparable to conventional coded OFDM with greatly reduced PAPR. Furthermore, results show that the PAPR performance obtained is very close to the 64-QAM single-carrier peak-power performance. So, the peak-power problem is solved for large constellations.

To My Parents and Brother

ACKNOWLEDGMENTS

I would like to thank my thesis adviser, Professor Douglas Jones, for his valuable advice, guidance and encouragement. I am especially thankful for our regular meetings and fruitful discussions.

I would also like to thank all those in the Electrical and Computer Engineering Department at Illinois who have made this a wonderful place to learn and work.

Finally, I would like to thank my parents for their continuous support.

TABLE OF CONTENTS

LIST OF TABLES

LIST OF FIGURES

CHAPTER 1

INTRODUCTION

The modulation known as orthogonal frequency-division multiplexing (OFDM) or discrete multi-tone modulation (DMT) has been widely popular among various wireline and wireless applications. The main advantage of OFDM systems over single-carrier modulation is that they enable high data-rate transmission and combat multipath fading by cross-channel forward error-correction (FEC) coding and a simple equalization scheme at the receiver. However, the approximately Gaussian-distributed output samples lead to a high peak-to-average power ratio (PAPR) of the transmit signal, which has become the major drawback of OFDM systems [1]. The high dynamic range of the OFDM signal requires an expensive high-power amplifier (HPA) with substantial back-off to avoid the nonlinear distortion caused by clipping, which results in low power efficiency.

Space-time-frequency (STF) block coding schemes take advantage of diversity at a transmitting station often without requiring any channel-state information (CSI); at the same time, when using orthogonal block codes, they allow simple decoding at the receiver station. However, they still have the high peak-to-average power ratio (PAPR) of OFDM, which requires high power-amplifier backoff and results in low efficiency [1]. We extend the efficient ACE smart gradient-project (SGP) method to space-time block coded (STBC), space-frequency block coded (SFBC) and V-BLAST OFDM systems. The proposed peak-power reduction method can be applied to any space-time-frequency (STF) block code, and its performance is bounded by the code structure. Simulations show PAPR reduction gains of 4.19 and 3.57 dB under QPSK for Alamouti STBC and SFBC, respectively.

The 2nd-generation terrestrial transmission system developed by the DVB

Project [2] is one of the most advanced digital video broadcasting systems in the world and uses OFDM for highly efficient use of terrestrial spectrum to deliver high-quality video, audio and data services to fixed, mobile and portable devices. The physical-layer structure of DVB-T2 includes a new technique, called rotated constellations [3], which provides extra diversity for difficult fading channels. It was believed that ACE cannot be used for rotated constellations [2], making the designer choose between diversity and peak-power reduction. Here, we extend ACE and the efficient smart gradient-project (SGP) method to rotated constellations and evaluate the performance for different original QAM constellation sizes. The results show near-optimum performance.

Tone injection is a PAPR reduction technique introduced by Tellado [4] that uses cyclic extensions of QAM constellations as degrees of freedom that can be exploited to lower the PAPR. When using this technique for coded-OFDM systems, the regular decoders are no longer optimal, resulting in a degradation of the BER performance. We provide a near-optimal way to design such decoders which can be easily adapted to convolutional, LDPC and turbo coding schemes. Simulation results for convolutional and LDPC coded-OFDM systems show BER performance comparable to conventional coded OFDM with greatly reduced PAPR.

CHAPTER 2

ORTHOGONAL FREQUENCY-DIVISION MODULATION

Before introducing the peak-power reduction techniques and the space-time-frequency block coding techniques that may be used with OFDM, it is necessary to introduce the motivation, intuition and mechanics behind OFDM.

2.1 Multipath Channels

Wireless channels are almost always characterized by multipath propagation. The basic wireless communication scenario at the physical layer consists of transmitting information wirelessly from point A to point B, at a specified reliability and rate. Challenges arise in a wireless environment due to unreliability factors such as scattering due to interferers (i.e., stationary or moving objects that affect the signal's path) and mobility of the transmitter and/or the receiver.

If every detail were known about the reflectors and absorbers present in the wireless environment, one could use Maxwell's equations to determine the exact propagation of electromagnetic signals. However, this model of a wireless channel is impractical and approximations can be made, since the transmitter and receiver antennas are usually separated by many wavelengths and far-field approximations can be used. Moreover, the model needs to be flexible enough to model more than one type of environment.

Using rays to model the electromagnetic signal, signals traveling through air can get attenuated and a propagation delay can be associated with each ray. The reflection each ray experiences by various objects before reaching the receiver can be modeled by receiving multiple copies of the transmitted signal at the receiver since

the signal is received by multiple paths, each of which is characterized by a different attenuation and delay. This is often called intersymbol interference (ISI). Additive noise at the receiver may also be incorporated in the model. A continuous-time fading channel model can be written as follows:

$$y(t) = \sum_i a_i(t)x(t - \tau_i(t)) + w(t) \tag{2.1}$$

where $a_i(t)$ and $\tau_i(t)$ denote the magnitude and delay associated with the ith path. Additive noise can be assumed to be white and complex Gaussian.

Doppler spread and multipath delay spread are quantities associated with a receiver at a given location, velocity and time. A statistical model of the channel is required to figure out how many taps are needed, how quickly they change and how much they vary. Each tap contains an aggregate of paths that fall within a sampling period. Assuming there are many statistically independent reflected and scattered paths with random amplitudes in the delay window corresponding to a single tap, we can model the channel taps as circularly symmetric complex Gaussian random variables (i.e., by the central limit theorem). Then, it can be shown that the magnitude of the channel coefficients follows a Rayleigh distribution. A discrete-time baseband model for the wireless channel can be written as an FIR filter [5]:

$$y[n] = \sum_l h_l[n]x[n - l] + w[n] \tag{2.2}$$

where $h_l[n] = \sum_i a_i(nT)e^{-j2\pi f_c \tau_i(nT)}\text{sinc}(l - \frac{\tau_i(nT)}{T})$ denotes the discrete-time channel's impulse response ($h_l[n]$ is the lth complex channel filter tap at time n) and f_c is the carrier frequency. Assuming the system clocks out information at discrete-time intervals T (i.e., where T is the symbol period), the delay τ_{max} of the longest path with respect to the earliest path is of critical importance since a received symbol tends to be affected by the previous τ_{max}/T symbols.

In this context, $h_l[n]$ is a circularly symmetric complex Gaussian random

variable ($h_l[n] \sim CN(0, \sigma_l^2)$). By this assumption, it can be shown [5] that the magnitude of the lth tap is Rayleigh distributed with density

$$\frac{x}{{\sigma_l}^2} e^{\frac{-x^2}{2{\sigma_l}^2}}, x \geq 0$$

This Rayleigh fading model is usually used for modeling scattering environments characterized by many small reflectors. However, if there is a direct line-of-sight (LOS) path with dominant energy and a large number of independent reflected and scattered paths, we can model the channel taps as

$$h_l[n] = \sqrt{\frac{\kappa}{\kappa+1}}\sigma_l e^{j\theta} + \sqrt{\frac{1}{\kappa+1}} CN(0, {\sigma_l}^2)$$

where κ (K-factor) is the ratio of energy in the LOS path to the energy in the scattered paths, the first term is due to the LOS path arriving with uniform phase θ, and the second term is due to the large number of independent paths. The magnitude of the channel taps then follows a Rician distribution.

2.2 Single-Carrier Systems

In a single-carrier system, bits are first converted to symbols and these symbols are pulse-shaped by a transmitter filter. Then, the signal is upconverted to a carrier frequency f_c and gets passed through the multipath channel. At the receiver, the signal first gets downconverted to baseband and a matched filter may be employed to maximize the signal-to-noise ratio (SNR) and help timing synchronization. The ISI induced by the channel is very difficult to cope with since the receiver has to pull all the weight to equalize the data by tracking the channel appropriately (i.e., with an adaptive LMS-like equalizer [5]). A single-carrier system's functional diagram is shown in Fig. 2.1.

As an example, if a wireless channel is characterized by a maximum channel delay of $\tau_{max} = 150$ μs, and we clock out symbols at a symbol rate of $R_s = 10$ Msymbols/s, then the receiver has to deal with an ISI of $\frac{\tau_{max}}{T} = 1500$

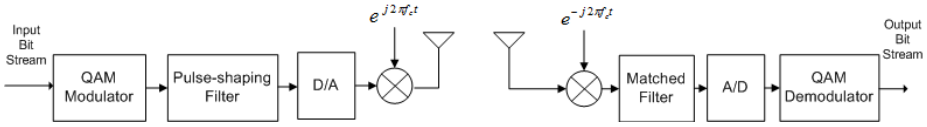

Figure 2.1: Basic diagram of a single-carrier system.

symbols!

2.3 Multicarrier Systems

Multicarrier systems are very different from single-carrier systems, in that they significantly reduce the ISI induced by the multipath channel. The original data stream of rate R is divided into N parallel lower-rate streams, each of rate R/N. Then, each data stream is modulated with a different frequency and the resulting signals are simultaneously transmitted. This is illustrated in Fig. 2.2.

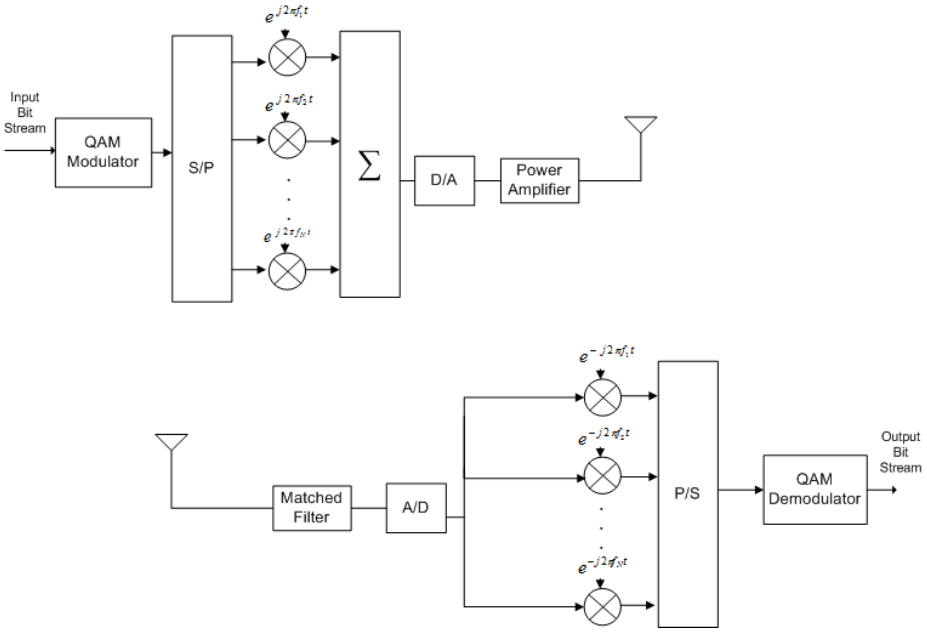

Figure 2.2: Basic diagram of a multicarrier system.

Using the same transmission scenario as in the single-carrier system, we can compute the ISI induced at the receiver for a multicarrier system of $N = 4092$:

$$\frac{\tau_{max}}{NT} \approx 0.366$$

Further increasing N lowers the ISI. Due to the little ISI, an equalizer is greatly simplified. In the light of multicarrier modulation, a practical multicarrier technique, known as OFDM, has arisen.

2.4 OFDM: A Balanced Approach

OFDM is a multicarrier transmission scheme that splits the available bandwidth into many subcarriers, each one modulated by a lower-rate stream. The carriers are closely spaced together and overlap one another in such a way that there is no interference between them. In other words, they are mutually orthogonal. One can think of these subcarriers as narrowband channels. Their mutual orthogonality stems from the fact that each carrier has an integer number of cycles over a symbol period, so each carrier has a null at the center frequency of each of the other carriers, resulting in no intercarrier interference. Each carrier in an OFDM system has a very narrow bandwidth (i.e., low symbol rate). Thus, the OFDM signal is robust against large delay spreads, since the channel's delay spread must be very long to cause significant ISI (i.e., $\tau_{max} > 500$ μs).

2.4.1 OFDM transmission

Essentially, OFDM converts the frequency-selective intersymbol interference (ISI) channel into a set of parallel additive white Gaussian noise (AWGN) channels. In other words, OFDM provides frequency diversity by modulating many low-rate streams simultaneously (and error correction capacity-achieving codes spread the individual bits) across a large bandwidth. The advantage is that if some particular range of frequencies is deeply faded, the overall signal can still be demodulated in a robust way.

Each subchannel is available a fraction $1/N$ of frequency and has a different SNR. The total power budget can be split across the subcarriers to maximize the rate of reliable communication when a subchannel operates at high SNR. The allocation strategy is as follows: the better the quality of a subchannel, the more power is allocated to it and the larger the corresponding data rate of reliable communication. This strategy is known as waterfilling [5]. At low SNR, the optimal allocation strategy tends to be uniform across all subcarriers. In situations in which the channel is unknown or may differ for different users (e.g., broadcast television), equal power allocation and FEC across frequencies is used to ensure reliable communication to all receivers.

To effectively combat multipath, OFDM also uses a cyclic prefix, which is also referred to as a guard interval (GI). The GI is inserted to mitigate ISI caused by the multipath channel. It is simply a copy of the last part of the OFDM symbol and is placed as a preamble to the original OFDM symbol. This makes the transmitted OFDM signal look periodic to the channel, thus allowing time for the multipath signals from the previous symbols to die away before the information from the current symbol is gathered. The GI plays two important roles: it provides protection against multipath, and allows for symbol time synchronization at the receiver. A disadvantage associated with it is the extra overhead it carries, which can be reduced by choosing larger OFDM block sizes. However, one cannot increase the OFDM block size indefinitely because it is upper-bounded by the coherence block length of the channel. Moreover, it is lower-bounded by the multipath delay spread. Windowing is applied after inserting the GI to reduce out-of-band radiation when the OFDM symbol exhibits a "discontinuous" start or end.

Figure 2.3 is a diagram of a typical uncoded OFDM transmitter.

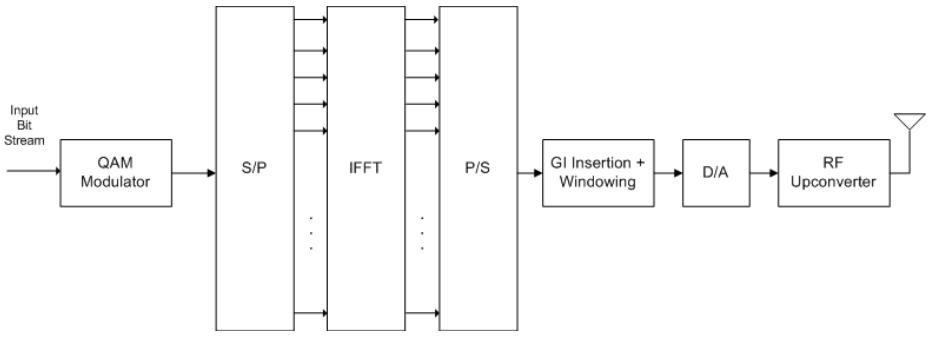

Figure 2.3: Typical OFDM transmitter.

D/A conversion produces the analog baseband signal which is then upconverted to RF and transmitted. As shown in the figure, OFDM modulation is performed by taking the inverse discrete Fourier transform (IDFT) of a block of N QAM data symbols. After the input bit stream gets modulated into blocks of QAM symbols (N symbols each), the jth complex-valued symbol vector $X_j = [X_{0,j}, X_{1,j}, ..., X_{N-1,j}]^T$ gets transmitted in parallel such that each QAM symbol modulates a different subcarrier from a total set of N subcarriers. These subcarriers are orthogonal, and the resulting discrete-time signal $x_j[n] = [x_{0,j}, x_{1,j}, ..., x_{N-1,j}]^T$ can be expressed as

$$x_j[n] = \frac{w[n]}{\sqrt{N}} \sum_{k=0}^{N-1} X_{k,j} e^{j2\pi kn/N} \tag{2.3}$$

where $w[n]$ is a discrete-time rectangular window with unity amplitude over the interval $[0, N-1]$. A cyclic prefix is then prepended to mitigate interblock interference and to aid the frequency-domain equalizer at the receiver. The signal can then be oversampled by a factor of L, and undergo some digital filtering. Digital-to-analog (D/A) conversion and analog filtering follow, and finally the signal is upconverted to a carrier frequency and fed into a high-power amplifier (HPA) which drives the antenna load. Due to the nature of OFDM modulation (taking a weighted sum of frequency-domain QAM symbols), the time-domain samples have a Gaussian-like distribution for large N (by the central limit theorem) and the HPA

needs to have a large dynamic range to support these large peaks at the tails of the distribution.

2.4.2 OFDM reception

The processing at the receiver is basically done by reversing the steps in the transmitter chain. Care should be taken to recover the timing after A/D conversion. A diagram of a typical uncoded OFDM receiver is shown in Fig. 2.4.

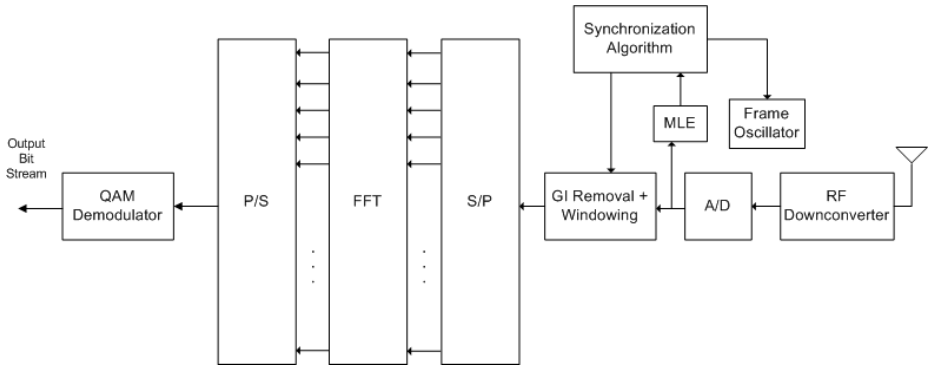

Figure 2.4: Typical OFDM receiver.

The symbol timing and carrier frequency offset between the transmitter and receiver must be estimated well enough such that the received signal constellation is not distorted too much (i.e., achieves a certain overall probability of error). The propagation channel, due to multipath fading and AWGN, causes a phase rotation of the individual subcarriers due to the complex channel gains. Carrier-frequency errors can reduce the amplitude of the desired signal and intercarrier interference (ICI) can arise.

An algorithm can be employed at the receiver which uses the cyclic prefixes emerging from the A/D converter and makes ML estimates to synchronize the channel. The start of OFDM frames needs to be correctly estimated for correct demodulation of the data (i.e., via a cross-correlation method with a pseudorandom sequence) using pilot sequences in the subcarriers. A frame oscillator can be used to correct the sampling frequency, and the GI can then be removed. Data demodulation follows.

CHAPTER 3

THE PEAK-POWER PROBLEM AND SOLUTIONS

A serious disadvantage of OFDM is its high peak-to-average power ratio (PAPR). This is due to the fact that many sinusoidal waves can add coherently (and destructively) to construct an OFDM signal. For example, when N identical signals are added with the same phase, the resulting signal has a peak power N times the average power. These large peaks saturate the power amplifier, which distorts the signal and also introduces out-of-band energy.

3.1 A Simple Approximation

The PAPR of an OFDM symbol block can be computed as

$$PAPR(\mathbf{x}) = \frac{\max_{0\leq k\leq N-1} |\mathbf{x}|^2}{E[|\mathbf{x}|_2^2]/N} \tag{3.1}$$

This is called digital PAPR. The equivalent analog formula is

$$PAPR(x(t)) = \frac{\max_{0\leq t\leq NT} |x(t)|^2}{E[|x(t)|^2]} = \frac{\max_{0\leq t\leq NT} |x(t)|^2}{\frac{1}{NT}\int_0^{NT} |x(t)|^2 dt} \tag{3.2}$$

where T is the symbol period and $x(t)$ is the baseband OFDM signal constructed from a certain block of N QAM symbols X_k given by

$$x(t) = \sum_{k=0}^{N-1} X_k e^{j2\pi f_n t}, 0 \leq t \leq NT, f_n = \frac{n}{NT} \tag{3.3}$$

Oversampling the discrete-time signal $x[n]$ to a factor of $L = 4$ is sufficient for capturing the continuous-time peaks, as discussed in [1], and to prevent large analog

'peak regrowth' at the D/A converter. To statistically evaluate the PAPR performance, the complementary cumulative distribution function (CCDF) of the PAPR of the OFDM time signals is used to describe the probability of exceeding a given threshold γ, i.e.,

$$CCDF(PAPR(\mathbf{x})) = Pr[PAPR(\mathbf{x}) > \gamma] \tag{3.4}$$

We can invoke the central limit theorem for a large number of subcarriers, in order to easily approximate the probability that the PAPR is larger than a specific level. Given a set of N constellation points $X[k], k = 0, 1, ..., N-1$, we can construct an OFDM signal to be transmitted using the orthonormal IDFT:

$$x[n] = \frac{1}{\sqrt{N}} \sum_{k=0}^{N-1} X[k] e^{j2\pi kn/N}$$

Assuming that $\Re(x[n])$ and $\Im(x[n])$ are pairwise-independent Gaussian i.i.d. (independent and identically distributed) random variables (with zero mean and variance 1/2), then the vector $\mathbf{R} = |\mathbf{x}|$ consists of N i.i.d. random variables with Rayleigh probability density function $f_R(r) = 2re^{-r^2} I_{\{r \geq 0\}}$. [1] Thus,

$$Pr[\max_{n=0,1,...,N-1} R[n] < \alpha] = (Pr[R < \alpha])^N = (1 - e^{-\alpha^2})^N$$

Using a random-variable transformation, it can be shown that
$K[n] = R[n]^2 \sim \exp(1)$ (i.e., $f_K(k) = e^{-k} I_{\{k \geq 0\}}$). Thus,

$$Pr[PAPR(\mathbf{x}) > \gamma] \approx 1 - (1 - e^{-\gamma})^N$$

This approximation is not exactly valid, mainly because when we choose symbols from a PSK or QAM constellation C, the pairwise independence assumption breaks down. Moreover, the maximum over the Nyquist samples of the signal can be significantly different from the continuous maximum. More

[1] Here, and throughout this thesis, $I_{\{\cdot\}}$ denotes the indicator function $I_{\{A\}} = 1$ if A is true and 0 otherwise.

sophisticated expressions can be computed by assuming that $\Re\{x[n]\}$ and $\Im\{x[n]\}$ are independent stationary bandlimited Gaussian processes with zero mean and variance $N_0/2$, and further assuming that the peaks are statistically mutually uncorrelated [6].

3.2 Some Proposed Solutions

Some proposed solutions to the PAPR problem include clipping, tone-reservation, partial transmit sequences, selected mapping, active constellation extension (ACE) and tone injection.

Probably the simplest technique to reduce the PAPR of a transmit OFDM signal is to clip the time-domain signal at some desired maximum level. Very large peaks tend not to occur very often, so the nonlinear effect of clipping the signal may not affect the bit error rate performance too much. Disadvantages of clipping include in-band distortion, which reduces the bit error rate performance, and out-of-band distortion, which violates regulatory constraints [7]. Filtering after clipping may also cause peak regrowth.

Tone-reservation schemes use some subcarriers as degrees of freedom to reduce the PAPR [8]. The subcarriers (tones) reserved for PAPR reduction do not carry data. A disadvantage of this scheme is the reduction of data bandwidth associated with its nature. Gradient-type algorithms can be used to quickly optimize the loading [9].

In partial transmit sequence (PTS) schemes, scrambling rotations are applied to groups of subcarriers in order to reduce the PAPR. The time signal with the lowest PAPR is selected. Major disadvantages of this technique include the extra side information required to be transmitted with the information signal in order to reverse the scrambling at the receiver, thus lowering the information data rate, and the increased computational complexity at the transmitter to arrive at a low-PAPR signal. Trying out all combinations at the transmitter is impractical, so various schemes tend to find smarter ways to do this (see [10]).

The selected mapping approach (SLM) consists of partitioning the subcarriers of an OFDM symbol into U blocks. Then, each block is multiplied by a rotation vector, all the rotated U data blocks are transformed into the time-domain by IFFT, and the vector with the lowest PAPR is selected for transmission [11]. The advantage of this method is that the CCDF of the PAPR signal gets raised to the power of M, where there are M candidate transmission signals. This advantage comes at the expense of an increase in computational complexity at the transmitter and extra side information associated with the best rotation transform for each of the U blocks that needs to be communicated to the receiver to reverse the rotation.

3.3 Active Constellation Extension

An elegant and robust PAPR reduction technique that has gained attention by the DVB-T2 and Wi-Max standards is active constellation extension (ACE). This technique does not sacrifice bandwidth or bit error rate performance. It is an iterative scheme that works by extending the outer QAM constellation points outwards to reduce peak levels. Moreover, a fast technique based on a gradient method exists which reduces the PAPR significantly in only a couple of iterations. Disadvantages of this technique include slightly increased transmit power and the fact that it becomes less effective for larger constellation sizes since the fraction of interior points to outer points increases. More details can be found in [1] and [12].

3.4 Tone Injection

Tone injection is another PAPR reduction technique introduced by Tellado [4] that extends the constellation space appropriately to reduce the peak power at a cost of slightly increasing the average power. Essentially, new degrees of freedom are created by cyclically extending the QAM constellation to allow for alternative encoding with lower PAPR. The name of the method is justified since the replacement of an original constellation point with one of the equivalent points in

the larger constellation corresponds to injecting a tone with proper frequency and phase in the OFDM symbol. Tuna's work [13] showed that single-carrier peak-power performance can be nearly achieved using a fast algorithm through an aggressive clipping approach. This thesis extends the practicality of this idea for coded OFDM systems.

CHAPTER 4

REVIEW OF DIVERSITY CODING

4.1 Diversity

The deleterious effects of intersymbol interference (ISI) and multipath fading can be effectively mitigated by exploiting *diversity* in wireless broadband communication systems, if certain mild conditions are satisfied. Diversity comes in three ways: time, frequency and space. The source of diversity comes from the random time- and/or frequency-varying nature of the wireless channels, essentially by correctly exploiting approximately independent paths the signal takes in a point-to-point setting. The idea is that if some signal paths are deeply faded, the signal may still have a high chance of survival by using other independent paths characterized by high SNR, thus greatly increasing the link's performance.

Temporal diversity can be achieved by repetition coding; for example, repeating the same symbol n times during different time instants, such that the receiver sees n different, independently faded copies of the same symbol. The way to do this is to transmit every coherence-time interval, so that each copy of the symbol sent "sees" a different channel. The disadvantage associated with this naive diversity technique is that the data rate gets reduced by a factor of n. Nevertheless, the WiMAX standard picks up time diversity by an FEC decoder (i.e., outer Reed-Solomon block code concatenated with an inner convolutional code) and appropriate interleaving.

Frequency diversity can also be achieved by repetition coding, but in a FDM fashion. By transmitting the same signal on different carrier frequencies (assuming their separation in frequency is at least as wide as the coherence bandwidth), each

copy sees a different channel and the receiver sees multiple independent copies of the same signal. OFDM is an excellent scheme to use for obtaining frequency diversity this way, especially when forward error-correction (FEC) coding is employed.

Spatial diversity is achieved by using multiple antennas at the transmitter and the receiver (i.e., MIMO). If these antennas are spread apart by a distance of several wavelengths (coherence distance), then the channel between each transmitter-receiver pair fades independently, enabling diversity. Receive antennas provide a diversity gain, but also a power gain. It is known that in an $M_T \times M_R$ MIMO system (M_T transmit and M_R receiver antennas), the maximum diversity gain is $M_T M_R$, assuming that the complex channel-fading coefficients between individual antenna pairs are i.i.d. Rayleigh-fading random variables [5].

4.2 Orthogonal Space-Time Block Codes

Space-time block codes (STBC) assume a flat fading environment. The assumption that the channel is approximately constant during the transmission of one block is also necessary. OFDM provides such an environment because it converts a frequency-selective channel into many flat-fading subchannels through the use of the IFFT and a cyclic-prefix insertion at each antenna. However, there is a catch; since the symbol duration of an OFDM symbol is significantly larger than that of a single-carrier system with the same bandwidth, the assumption that the channel is approximately constant during the transmission of one block should be carefully monitored. This is one of the reasons why the two-transmit-antenna Alamouti scheme [14] is so popular: it does not sacrifice bandwidth or decoder complexity, and achieves a full transmit diversity gain without the need for channel-state information, and the above-mentioned assumption is easily satisfied for most channels.

The assumption that the channel is approximately constant during the transmission of a space-time block is challenged in wireless environments characterized by high Doppler shifts and high vehicular speeds. OFDM provides

high spectral efficiency and degrees of freedom in spreading the time dimension of STBCs over subcarriers.

The code rate associated with each STBC design is directly associated with delay and will be defined in the next section. The closer the code rate is to unity (which is known to be achieved only by the Alamouti scheme [14] for complex orthogonal designs [15]), the less the delay. If the code rate is exactly one, then there is no propagation delay induced by the diversity-coding scheme.

4.2.1 Theory of amicable orthogonal designs

Linear STBCs are characterized by the following structure:

$$\mathbf{X} = \sum_{n=1}^{k} \Re(s_n)\mathbf{A}_n + j\Im(s_n)\mathbf{B}_n \tag{4.1}$$

where $\{s_n\}$ is a set of k symbols chosen from a constellation C to be used in the code matrix $\mathbf{X}$, and $\mathbf{A}_n, \mathbf{B}_n$ are chosen complex code matrices of size $M_T \times p$. Because k complex symbols are transmitted over p transmission periods, the code rate is given by

$$R = \frac{k}{p} \tag{4.2}$$

Orthogonal STBCs are an important class of linear STBCs. They guarantee that coherent maximum-likelihood (ML) detection of different symbols is decoupled and achieves a diversity of the order $M_T M_R$. Orthogonal STBCs further obey the following unitary property:

$$\mathbf{X}\mathbf{X}^H = c\sum_{n=1}^{k} |s_n|^2 \mathbf{I} \tag{4.3}$$

where c is an arbitrary scaling factor. The link joining (4.1) and (4.3) is a set of conditions on matrices $\mathbf{A}_n, \mathbf{B}_n$ and are outlined in Theorem 4.2.1 below.

Theorem 4.2.1 (Relation between orthogonal STBCs and amicable orthogonal

designs [16]) *Let* $\boldsymbol{X}$ *be a matrix as defined in (4.1). Then, (4.3) is satisfied for all complex* $\{s_n\}$ *iff* $\boldsymbol{A}_n, \boldsymbol{B}_n$ *is an amicable orthogonal design; i.e.:*

$$\begin{aligned}
\boldsymbol{A}_n \boldsymbol{A}_n{}^H &= \boldsymbol{I} \\
\boldsymbol{B}_n \boldsymbol{B}_n{}^H &= \boldsymbol{I} \\
\boldsymbol{A}_n \boldsymbol{A}_m{}^H &= -\boldsymbol{A}_m \boldsymbol{A}_n{}^H, n \neq m \\
\boldsymbol{B}_n \boldsymbol{B}_m{}^H &= -\boldsymbol{B}_m \boldsymbol{B}_n{}^H, n \neq m \\
\boldsymbol{A}_n \boldsymbol{B}_m{}^H &= \boldsymbol{B}_m \boldsymbol{A}_n{}^H
\end{aligned} \tag{4.4}$$

for $n = 1, ..., k$, *and* $m = 1, ..., k$.

Proof The proof of this theorem is included in [17]. ∎

As a simple illustration, one can derive the famous Alamouti STBC [14]

$$X = \begin{bmatrix} s_1 & -s_2^* \\ s_2 & s_1^* \end{bmatrix}$$

via the following code matrices and using (4.1)

$$\mathbf{A}_1 = \begin{bmatrix} 1 & 0 \\ 0 & 1 \end{bmatrix}$$

$$\mathbf{A}_2 = \begin{bmatrix} 0 & -1 \\ 1 & 0 \end{bmatrix}$$

$$\mathbf{B}_1 = \begin{bmatrix} 1 & 0 \\ 0 & -1 \end{bmatrix}$$

$$\mathbf{B}_2 = \begin{bmatrix} 0 & 1 \\ 1 & 0 \end{bmatrix}$$

The rate of this code is unity (full rate). Another example is the 3/4 rate sporadic code [15] for four transmit antennas

$$X = \begin{bmatrix} s_1 & -s_2^* & \frac{s_3^*}{\sqrt{2}} & \frac{s_3^*}{\sqrt{2}} \\ s_2 & s_1^* & \frac{s_3^*}{\sqrt{2}} & -\frac{s_3^*}{\sqrt{2}} \\ \frac{s_3}{\sqrt{2}} & \frac{s_3}{\sqrt{2}} & \frac{(-s_1-s_1^*+s_2-s_2^*)}{2} & \frac{(s_2+s_2^*+s_1-s_1^*)}{2} \\ \frac{s_3}{\sqrt{2}} & -\frac{s_3}{\sqrt{2}} & \frac{(-s_2-s_2^*+s_1-s_1^*)}{2} & -\frac{(s_1+s_1^*+s_2-s_2^*)}{2} \end{bmatrix}$$

which can be constructed via the following unitary code matrices and using (4.1)

$$\mathbf{A}_1 = \begin{bmatrix} 1 & 0 & 0 & 0 \\ 0 & 1 & 0 & 0 \\ 0 & 0 & -1 & 0 \\ 0 & 0 & 0 & -1 \end{bmatrix}$$

$$\mathbf{A}_2 = \begin{bmatrix} 0 & -1 & 0 & 0 \\ 1 & 0 & 0 & 0 \\ 0 & 0 & 0 & 1 \\ 0 & 0 & -1 & 0 \end{bmatrix}$$

$$\mathbf{A}_3 = \frac{1}{\sqrt{2}} \begin{bmatrix} 0 & 0 & 1 & 1 \\ 0 & 0 & 1 & -1 \\ 1 & 1 & 0 & 0 \\ 1 & -1 & 0 & 0 \end{bmatrix}$$

$$\mathbf{B}_1 = \begin{bmatrix} 1 & 0 & 0 & 0 \\ 0 & -1 & 0 & 0 \\ 0 & 0 & 0 & 1 \\ 0 & 0 & 1 & 0 \end{bmatrix}$$

$$\mathbf{B}_2 = \begin{bmatrix} 0 & 1 & 0 & 0 \\ 1 & 0 & 0 & 0 \\ 0 & 0 & 1 & 0 \\ 0 & 0 & 0 & -1 \end{bmatrix}$$

$$\mathbf{B}_3 = \frac{1}{\sqrt{2}} \begin{bmatrix} 0 & 0 & -1 & -1 \\ 0 & 0 & -1 & 1 \\ 1 & 1 & 0 & 0 \\ 1 & -1 & 0 & 0 \end{bmatrix}$$

According to the Alamouti scheme [14], the encoder takes a block of two QAM symbols s_1 and s_2 and assigns it to the two transmit antennas according to the following code matrix

$$X_A = \begin{bmatrix} s_1 & -s_2^* \\ s_2 & s_1^* \end{bmatrix}$$

where the ith column represents the ith transmission period and the jth row corresponds to the jth antenna's symbols. In this thesis, simulation results are shown for the Alamouti code and the following well-known orthogonal codes designed for four transmit antennas [15], with code rates 1/2 and 3/4, respectively:

$$X_B = \begin{bmatrix} s_1 & -s_2 & -s_3 & -s_4 & s_1^* & -s_2^* & -s_3^* & -s_4^* \\ s_2 & s_1 & s_4 & -s_3 & s_2^* & s_1^* & s_4^* & -s_3^* \\ s_3 & -s_4 & s_1 & s_2 & s_3^* & -s_4^* & s_1^* & s_2^* \\ s_4 & s_3 & -s_2 & s_1 & s_4^* & s_3^* & -s_2^* & s_1^* \end{bmatrix}$$

$$X_C = \begin{bmatrix} s_1 & 0 & s_2 & -s_3 \\ 0 & s_1 & s_3^* & s_2^* \\ -s_2^* & -s_3 & s_1^* & 0 \\ s_3^* & -s_2 & 0 & s_1^* \end{bmatrix}$$

4.2.2 Maximum-likelihood detection

An important property of orthogonal STBCs is the fact that maximum-likelihood (ML) detection can be achieved at the receiver separately for each symbol. If the channel is not constant during the transmission of a block, then the orthogonality is distorted and intersymbol interference occurs.

Assuming a quasi-static channel, the received signal at the jth receive antenna can be expressed as

$$r_j(t) = \sum_{i=1}^{M_T} h_{ij} x_i(t) + n_j(t), \;\; j = 1, ..., M_R \tag{4.5}$$

where h_{ij} is the complex channel gain from the ith transmit antenna to the jth receive antenna, $x_i(t)$ are the signals transmitted simultaneously from the transmit antennas at each time slot t, and $n_j(t)$ denotes the zero-mean independent complex Gaussian noise samples with variance $M_T/(2 \text{ SNR})$ per complex dimension. This is true assuming that the average symbol energy is normalized to unity, and thus the average power of the received signal at each receive antenna is M_T and the signal-to-noise ratio is SNR.

Assuming coherent processing at the receiver, the following metric is minimized over all transmit signals $x_i(t)$:

$$\sum_{t=1}^{p} \sum_{j=1}^{M_R} |r_j(t) - \sum_{i=1}^{M_T} h_{ij} x_i(t)|^2 \tag{4.6}$$

where p is the number of transmission periods.

As a simple concrete example, let us consider the decoding of symbols s_1 and s_2 for the Alamouti scheme ($p = 2$) under flat-fading channel conditions. At the first transmission period, the encoder selects and transmits two complex symbols s_1 and s_2 from a constellation C, and at the second transmission period, it transmits $-s_2^*$ and s_1^*, from the first and second transmit antennas respectively.

To perform ML detection, the following decision metric is minimized over all possible symbols s_1 and s_2:

$$\sum_{j=1}^{M_R} |r_j(1) - (h_{1j}s_1 + h_{2j}s_2)|^2 + |r_j(2) - (h_{1j}(-s_2^*) + h_{2j}s_1^*)|^2 \tag{4.7}$$

Expanding, simplifying and getting rid of terms that do not depend on s_1 and s_2, the following metric is minimized over all possible s_1 and s_2:

$$\begin{aligned}\sum_{j=1}^{M_R} \Big[& - r_j(1)h_{1j}^* s_1^* - r_j(1)h_{2j}^* s_2^* - r_j(1)^* h_{1j}s_1 - r_j(1)^* h_{2j}s_2 \\ & + r_j(2)h_{1j}^* s_2 - r_j(2)h_{2j}^* s_1 + r_j(2)^* h_{1j}s_2^* - r_j(2)^* h_{2j}s_1^* \Big] \\ & + |s_1|^2 \sum_{j=1}^{M_R}\sum_{i=1}^{2} |h_{ij}|^2 + |s_2|^2 \sum_{j=1}^{M_R}\sum_{i=1}^{2} |h_{ij}|^2 \end{aligned} \tag{4.8}$$

The above metric can be decomposed into two parts. The first only involves s_1

$$\sum_{j=1}^{M_R} -r_j(1)h_{1j}^* s_1^* - r_j(1)^* h_{1j}s_1 - r_j(2)h_{2j}^* s_1 - r_j(2)^* h_{2j}s_1^* + |s_1|^2 \sum_{j=1}^{M_R}\sum_{i=1}^{2} |h_{ij}|^2 \tag{4.9}$$

and the second involves only s_2

$$\sum_{j=1}^{M_R} -r_j(1)h_{2j}^* s_2^* - r_j(1)^* h_{2j}s_2 + r_j(2)h_{1j}^* s_2 + r_j(2)^* h_{1j}s_2^* + |s_2|^2 \sum_{j=1}^{M_R}\sum_{i=1}^{2} |h_{ij}|^2 \tag{4.10}$$

Thus, minimizing (4.7) is equivalent to separately minimizing (4.9) and (4.10).

It turns out that (4.9) and (4.10) can be further simplified:

$$\left|\left[\sum_{j=1}^{M_R} r_j(1)h_{1j}^* + r_j(2)^* h_{2j}\right] - s_1\right|^2 + \left(\sum_{j=1}^{M_R}\sum_{i=1}^{2}|h_{ij}|^2 - 1\right)|s_1|^2 \tag{4.11}$$

$$\left|\left[\sum_{j=1}^{M_R} r_j(1)h_{2j}^* - r_j(2)^* h_{1j}\right] - s_2\right|^2 + \left(\sum_{j=1}^{M_R}\sum_{i=1}^{2}|h_{ij}|^2 - 1\right)|s_2|^2 \tag{4.12}$$

To summarize, the simple linear ML decoding strategy amounts to minimizing (4.11) for decoding s_1 and (4.12) for s_2. For equal-energy symbols (e.g., PSK), it suffices to compute

$$\widehat{s_1} = \arg\min_{s_1 \in C}\left|\left[\sum_{j=1}^{M_R} r_j(1)h_{1j}^* + r_j(2)^* h_{2j}\right] - s_1\right|^2 \tag{4.13}$$

$$\widehat{s_2} = \arg\min_{s_2 \in C}\left|\left[\sum_{j=1}^{M_R} r_j(1)h_{2j}^* - r_j(2)^* h_{1j}\right] - s_2\right|^2 \tag{4.14}$$

It is evident that the detection of s_1 and s_2 is equivalent to applying a matched filter. Thus, we observe that the Alamouti scheme provides full overall diversity of order $2M_R$ when using M_R receive antennas [14], [15]. This ML detection technique can be generalized for other orthogonal STBCs [18].

4.3 Orthogonal Space-Frequency Block Codes

The use of space-time block codes is questioned in fast-fading environments, and it is necessary to think of a different diversity strategy. Space-frequency block codes (SFBC) are a simple and viable solution to this type of fading environment.

4.3.1 A simple extension

The coding in space-time block codes takes place by coding across the time and antenna dimensions. SFBCs achieve diversity by coding across neighboring

frequency bins and antennas, rather than on the same subcarrier of subsequent OFDM symbols (i.e., as in STBC), thus reducing the transmission delay. SFBCs tend to suffer under severe frequency-selective conditions because the channel tap gains might vary across neighboring subcarriers.

CHAPTER 5

PEAK-POWER REDUCTION FOR STBC/SFBC/V-BLAST MIMO-OFDM VIA ACE

One can exploit time, frequency and spatial diversity by jointly designing a space-time-frequency block code which codes across multiple OFDM symbols, subcarriers and antennas. In an OFDM system, one can use a convolutional code and a random interleaver to obtain time and frequency diversity and an STBC to obtain spatial diversity. This section will show how the active constellation extension (ACE) method for peak-power reduction can be extended to such codes.

5.1 ACE-SGP STBC MIMO-OFDM Algorithm

5.1.1 STBC MIMO-OFDM

The simplest 2×2 STBC with full diversity was first introduced by Alamouti in [14]. The encoder takes a block of two QAM symbols X_1 and X_2 and assigns it to the two transmit antennas according to the following code matrix:

$$X_A = \begin{bmatrix} X_1 & X_2 \\ -X_2^* & X_1^* \end{bmatrix}$$

where the ith row represents the ith transmission period and the jth column corresponds to the jth antenna's symbols.

We also show simulation results for the following well-known orthogonal codes designed for four transmit antennas, with code rates 1/2 and 3/4, respectively:

$$X_B = \begin{bmatrix} X_1 & -X_2 & -X_3 & -X_4 & X_1^* & -X_2^* & -X_3^* & -X_4^* \\ X_2 & X_1 & X_4 & -X_3 & X_2^* & X_1^* & X_4^* & -X_3^* \\ X_3 & -X_4 & X_1 & X_2 & X_3^* & -X_4^* & X_1^* & X_2^* \\ X_4 & X_3 & -X_2 & X_1 & X_4^* & X_3^* & -X_2^* & X_1^* \end{bmatrix}^T$$

$$X_C = \begin{bmatrix} X_1 & 0 & X_2 & -X_3 \\ 0 & X_1 & X_3^* & X_2^* \\ -X_2^* & -X_3 & X_1^* & 0 \\ X_3^* & -X_2 & 0 & X_1^* \end{bmatrix}^T$$

5.1.2 STBC MIMO-OFDM gradient-project algorithm

The solution to the peak-to-average power (PAPR) reduction problem can be obtained with a fast gradient-project method, where only a couple of iterations are needed to considerably reduce the PAPR. A detailed discussion of the ACE-SGP algorithm can be found in [12].

Each symbol block appears alone on each antenna in each time period, so the peak power is the maximum of the individual blocks $\pm X_i$, $\pm X_i^*$, which can be minimized independently using the SISO ACE algorithm. Due to the structure of orthogonal space-time block codes, the SISO ACE-SGP algorithm need only be applied for the first transmission period, since it can be proven that complex sequences $X[k]$ and $\pm X^*[k]$ exhibit the same PAPR properties. This proof is trivial and follows below.

Theorem 5.1.1 *Complex sequences* $\{X[k] : 1 \leq k \leq N\}$ *and* $\{\pm X^*[k] : 1 \leq k \leq N\}$ *exhibit the same PAPR properties.*

Proof From the discrete Fourier transform (DFT) properties, if $x[(n)] \overset{\mathfrak{F}}{\leftrightarrow} X[k]$, then it also holds that $x^*[(-n)_{modN}] \overset{\mathfrak{F}}{\leftrightarrow} X^*[k]$ (where $*$ denotes complex-conjugate).

Let us denote the first discrete-time sequence as $x_1[n] = x[n]$ and the second as $x_2[n] = x^*[(-n)_{modN}]$. Recalling the digital PAPR definition (3.1), it suffices to show that $\max_n |x_1[n]|^2 = \max_n |x_2[n]|^2$ and $E[|x_1|_2^2] = E[|x_2|_2^2]$ in order for the complex sequences $X[k]$ and $\pm X^*[k]$ to have the same PAPR. First, note that $\max_n |x_1[n]|^2 = \max_n |x[n]|^2$, where $|x[n]|^2 = x[n]x^*[n]$. Then, we also have $\max_n |x_2[n]|^2 = \max_n |\pm x^*[(-n)_{modN}]|^2 = \max_n |x[(-n)_{modN}]|^2$. Evidently, $\max_n |x_1[n]|^2 = \max_n |x_2[n]|^2$ because $x[(-n)_{modN}]$ is just a circularly flipped version of $x[n]$, and the first part is proved. Second, note that $E[|x|_2^2] = \sum_{n=0}^{N-1} |x[n]|^2 = \frac{1}{N} \sum_{k=0}^{N-1} |X[k]|^2$, where the second equality follows from Parseval's theorem. Then, since $|X[k]|^2 = |\pm X^*[k]|^2$, we have $|X_1[k]|^2 = |X_2[k]|^2$ and by Parseval's theorem, we conclude that $E[|x_1|_2^2] = E[|x_2|_2^2]$. A similar version of this proof can be written for analog PAPR. ∎

Therefore, we only need to perform ACE-SGP processing on each SISO block independently, obtaining the minimum PAPR time-domain signal ready to transmit after adding the cyclic prefix for the first transmission period. To obtain the time-domain signals for the rest of the transmission periods, the scaling and conjugate DFT properties can be used to avoid the unnecessary IFFT operations for the remaining transmission periods across all transmit antennas:

$$x^*[(-n)_{modN}] \overset{\mathfrak{F}}{\leftrightarrow} X^*[k]$$

This property is especially useful for lower-rate codes, such as X_C.

5.2 ACE-SGP SFBC MIMO-OFDM Algorithm

5.2.1 SFBC MIMO-OFDM

Space-frequency block coding is another way to obtain diversity in order to improve the performance when employing multiple antennas at the transmitter and the receiver, particularly when there is frequency-selective fading. Coding occurs across

adjacent subcarriers of the same OFDM symbol rather than on the same subcarrier of subsequent OFDM symbols (STBC), thus reducing the transmission delay.

5.2.2 SFBC MIMO-OFDM gradient-project algorithm

The main idea of the ACE-SGP algorithm is to look at the residual clipped-off signal and project it onto the space of allowable extension vectors. The result is a peak-reduction signal scaled by an optimal step size subtracted from the time-domain signal. For space-time-frequency (STF) block codes, to correctly decode the signal, we project the residual clipped-off signal into the space of allowable space-time-frequency block code extensions, which depends on the code being used.

In general, the set of possible ACE vectors will be convex. The three convex sets are:

1. The set S_A consisting of all vectors $\mathbf{y} \in \mathbb{R}^N$ such that $||\mathbf{y}||_\infty \leq A$ for some positive constant A.

2. The set S_C, an N-dimensional subspace of $\mathbb{R}^N$, consisting of all vectors $\mathbf{y}$ with FFT $\mathbf{Y}$ that satisfy the data-dependent ACE restrictions.

3. The set S_B, a K-dimensional ($K = M_T p$, where p is the number of transmission periods and M_T is the number of transmit antennas) subspace of $\mathbb{R}^N$, consisting of all vectors $\mathbf{x}$ that yield the largest allowable ACE extension while maintaining the STF block code linear decoding properties.

Below is a basic pseudocode for an STF block code OFDM algorithm based on the gradient-project method.

1. Starting with the input bit stream, break it up into blocks of size N for parallel transmission, where there are N subchannels total. Consider transmission of p OFDM blocks per antenna. Perform M-QAM modulation to obtain the frequency-domain symbols, X_k.

2. Add transmit diversity by performing space-time-frequency block coding and determine the allowable extensions for each subchannel.

3. Take the IFFT for each antenna's signal to construct the time signal, $x^0[n,l]_t$, for each antenna l (n is the subchannel index, l is the antenna index, and t is the transmission period index). Set $i = 0$.

4. Clip any $|x^i[n,l]_t| \geq A$ in magnitude for some clip level A (i.e., project onto S_A) to obtain

$$\bar{x}[n,l]_t = \begin{cases} x^i[n,l]_t & |x^i[n,l]_t| \leq A \\ Ae^{j\theta[n,l]_t} & |x^i[n,l]_t| > A \end{cases} \tag{5.1}$$

where

$$x^i[n]_t = |x^i[n,l]_t| e^{j\theta[n,l]_t} \tag{5.2}$$

5. Compute the clipped signal portion (nonzero only at clipped samples)

$$c_{clip}[n,l]_t = \bar{x}[n,l]_t - x^i[n,l]_t \tag{5.3}$$

6. Apply an FFT to each antenna's clipped signal to obtain $C_{clip}[k,l]_t$.

7. Keep only the components of $C_{clip}[k,l]_t$ which are acceptable extension directions for the given subchannel constellations and set all remaining elements to zero (i.e., project onto S_C).

8. Apply the STF block code constraint (i.e., project onto S_B) by taking the maximum ACE extension and enforcing it on each block according to the code matrix.

9. Apply an IFFT to obtain $c[n,l]_t$.

10. Determine a step size μ according to the smart gradient criterion (i.e., for quick convergence, see [12])

$$x^{i+1}[n,l]_t = x^i[n,l]_t + \mu[l]_t c[n,l]_t \tag{5.4}$$

11. If an acceptable PAPR or a maximum iteration count has not been reached, update $i = i + 1$ and return to Step 4. Otherwise, stop PAPR reduction.

This algorithm's complexity is $O(M_T NL \log NL)$ (for each iteration) due to the oversampled IFFT/FFT operations. The algorithm converges sufficiently after 3 to 4 iterations. The algorithm described here can be applied to a general STF block code and it greatly simplifies for orthogonal STBC/SFBCs (i.e., as in Section 5.1.2).

5.3 ACE-SGP V-BLAST MIMO-OFDM Algorithm

Unlike STBCs, V-BLAST has a multiplexing gain but lacks a diversity gain [19]. Because independent data streams are sent on the different transmit antennas, the ACE-SGP algorithm can be applied on each antenna's time signal independently, like in the SISO case described in great detail in [12].

While space-time-frequency block codes aim to achieve reliable communication of one symbol per channel use and maximize the diversity gain, a scheme called the Vertical Bell Labs Space Time Architecture (V-BLAST) aims to increase the rate of the system by communicating M_T symbols per channel use (where there are M_T transmit antennas), achieving a multiplexing gain. Thus, there is a tradeoff between multiplexing and diversity gains which limits the overall theoretical performance of a MIMO system.

5.3.1 Diversity

The source of the data rate increase in the V-BLAST system comes from the spatial dimension. Since information is carried through spatial channels, diversity is achieved through space assuming the signal paths between transmit-receiver antenna pairs fade independently.

5.3.2 Detection algorithm

In a V-BLAST system, there needs to be a rich scattering environment to fully exploit the multipath. For this reason, there are typically more receive than transmit antennas. Denoting the $M_R \times M_T$ channel matrix as H (assuming the channel is time-invariant), the (i, j)th element of the matrix contains the complex tap gain from the jth transmit antenna to the ith receive antenna. Let us suppose that we want to transmit a vector $\mathbf{x}$ of M_T symbols chosen from a constellation C at a certain time slot: $\mathbf{x} = [x_1, x_2, ..., x_{M_T}]^T$ (i.e., transmitting one symbol per antenna simultaneously). The received $M_R \times 1$ vector can be written as

$$\mathbf{r}(1) = H\mathbf{x} + \mathbf{n} \tag{5.5}$$

where $\mathbf{n}$ denotes i.i.d. wide-sense stationary noise with variance σ^2. Our goal is to correctly decode the symbols contained in vector $\mathbf{x}$. To detect $\mathbf{x}$, linear combinatorial nulling can be used in combination with successive cancellation; the idea is to try to decode one substream, while treating the rest of the substreams as interference, then subtract the decoded substream from the received vector and repeat the process until all substreams have been decoded. This successive interference cancellation procedure provides superior performance compared to simple linear nulling because the subtraction of interference of the already decoded symbols changes the received vector into a modified vector with less interference. Because successive interference cancellation is a nonlinear technique, the order in which the components of $\mathbf{x}$ are detected is important for the system's performance. The general detection procedure can be found in [19].

The ACE method offers increased margins, guaranteeing lower error rates under AWGN conditions [12]. We claim that there is virtually no performance loss when using ACE for V-BLAST OFDM systems. This is because the V-BLAST detection algorithm is essentially a bank of linear minimum mean-square error (MMSE) receivers with successive cancellation (SIC) [5]. Due to the nature of the ACE extensions, error propagation in the SIC tends to be slightly more severe when

it occurs. This problem may be mitigated if the constellation points can be mapped back to their original locations prior to V-BLAST detection (i.e., via slicing and clustering in the constellation domain). However, slicing and clustering this way quantizes the performance of the V-BLAST detector and further degrades BER significantly. Since the BER increase is fairly small, one can increase the link's SNR by boosting the transmit power slightly, obtaining the target probability of error and a net PAPR gain slightly smaller than the simulations show.

5.4 Simulation results

Results of the ACE-SGP algorithm for STBC and SFBC MIMO-OFDM are shown in Fig. 5.1. The algorithm was tested for a complex-baseband STBC OFDM two-antenna system with $N = 256$ subchannels employing QPSK using 10^5 randomly generated OFDM symbol blocks. A level A of 4.0 dB above the average power was used to obtain the clipped signal to project onto the space of allowable extension vectors, and an upsampling factor of $L = 4$ was used to approximate analog PAPR reduction. Failure to process oversampled digital signals leads to large 'peak regrowth' at the D/A converter. Oversampling was performed by frequency-domain zero-padding and using oversampled IFFT operations.

As shown in Fig. 5.1, for Alamouti STBC, looking at a 10^{-3} symbol clip probability level, the third iteration achieves a PAPR reduction of approximately 4.19 dB. Further iterations provide negligible performance increases. Similarly, for Alamouti SFBC, a PAPR reduction of 3.57 dB is achieved in the third iteration.

Tables 5.1 and 5.2 [2] summarize the PAPR reduction gains obtained using a 256-subcarrier MIMO-OFDM system when looking at a 10^{-3} symbol clip probability. An upsampling factor $L = 4$ and the clipping levels, A, used were 4.0, 5.0, and 5.0 dB above the average power, for codes X_A, X_B, and X_C, respectively.

[2] In Tables 5.1, 5.2 and 5.3, ΔP_4 denotes the reduction in PAPR for 4-QAM, ΔP_{16} denotes the reduction in PAPR for 16-QAM, ΔP_{64} denotes the reduction in PAPR for 64-QAM and P^0 denotes the initial PAPR.

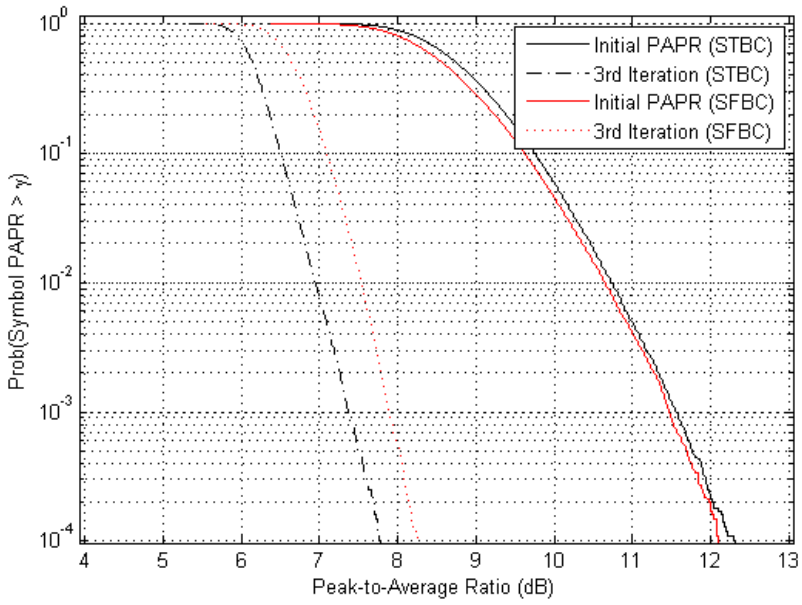

Figure 5.1: CCDF results with 2-Tx antenna STBC/SFBC using 256 subcarriers employing QPSK.

In each simulation run, 100,000 OFDM blocks were used.

Table 5.3 summarizes the PAPR reduction gains obtained for V-BLAST, which are all obtained for a 256 subcarrier MIMO-OFDM system when looking at a 10^{-3} symbol clip probability. Clipping levels A of 4.0 and 6.0 dB above the average power were used for two and four transmit antennas, respectively (with $L = 8$). Larger PAPR reduction gains were obtained for the V-BLAST MIMO-OFDM systems than the STBC/SFBC cases because there is no constraint across the signals being sent out from the antennas (i.e., independent streams).

Table 5.1: PAPR Reduction Results for Different Space-Time Block Codes and Modulation Types

STBC	ΔP_4 (dB)	ΔP_{16} (dB)	ΔP_{64} (dB)	P^0 (dB)
X_A	4.19	2.61	1.46	11.55
X_B	3.96	2.30	1.08	11.74
X_C	2.32	0.78	0.20	12.85

Table 5.2: PAPR Reduction Results for Different Space-Frequency Block Codes and Modulation Types

SFBC	ΔP_4 (dB)	ΔP_{16} (dB)	ΔP_{64} (dB)	P^0 (dB)
X_A	3.57	2.52	1.65	11.46
X_B	2.27	1.60	1.28	11.80
X_C	2.28	0.88	0.52	11.57

Table 5.3: PAPR Reduction Results for V-BLAST under Different Numbers of Antennas and Modulation Types

M_T (antennas)	ΔP_4 (dB)	ΔP_{16} (dB)	ΔP_{64} (dB)	P^0 (dB)
2	4.04	2.50	1.27	11.52
4	4.44	3.04	1.88	11.69

CHAPTER 6

PEAK-POWER REDUCTION FOR ROTATED CONSTELLATIONS VIA ACE

The efficient smart gradient-project (SGP) method of ACE can be extended to rotated constellations for broadcast SISO-OFDM systems.

6.1 Rotated Constellations

The 2nd-generation terrestrial transmission system developed by the DVB Project [2] is one of the most advanced digital video broadcasting systems in the world and uses OFDM for highly efficient use of terrestrial spectrum to deliver high-quality video, audio and data services to fixed, mobile and portable devices. The physical-layer structure of DVB-T2 includes a new technique, called rotated constellations [3], which provides extra diversity for difficult fading channels.

Rotated constellations is a method of obtaining frequency diversity in OFDM transmissions to combat frequency-selective fading. The motivation behind this idea is to combat fading channels more efficiently and exploit higher code rates. With rotated constellations, two pulse-amplitude modulated (PAM) axes of rotated QAM are sent simultaneously in *different* OFDM channels (via cyclic delay), which in turn occupy different positions in time and frequency [2], [3]. This technique effectively reduces the probability that any symbol is entirely lost.

The forward mapping of the regular QAM constellation into a rotated constellation is implemented in the DVB-T2 standard as follows. Let the jth complex-valued symbol vector $X_j = [X_{0,j}, X_{1,j}, ..., X_{N-1,j}]^T$ be the jth N-channel-long FEC block outputted from the FEC LDPC encoder. This block's real and imaginary parts are rotated by a constant rotation angle depending on the

constellation size, and the imaginary part is cyclically delayed by one channel within every FEC block.

The output channels are given by

$$G_{0,j} = \Re\{R_{\phi^\circ} X_{0,j}\} + j\Im\{R_{\phi^\circ} X_{N-1,j}\} \tag{6.1}$$

$$G_{k,j} = \Re\{R_{\phi^\circ} X_{k,j}\} + j\Im\{R_{\phi^\circ} X_{k-1,j}\}, \text{for } k = 1, 2, ..., N-1 \tag{6.2}$$

where the rotation phase is $R_{\phi^\circ} = e^{\frac{j2\pi\phi^\circ}{360}}$. The rotation angles chosen for different constellation sizes can be found in [2] and are also shown in Table 6.1. These angles are based on compromises between degrees of selectivity in various fading channels. All constellation sizes have non-uniform PAM projections, except for the 256-QAM case. The only extra price is the slight receiver complexity for the metric calculation. Bit decisions can be made directly by computing the bitwise log-likelihood ratios.

Table 6.1: Rotation Angles for Different Modulation Types

Constellation	4-QAM	16-QAM	64-QAM	256-QAM
Rotation Angle	29°	16.8°	8.6°	$Tan^{-1}(\frac{1}{16})$

It was believed that ACE cannot be used for rotated constellations [2], making the designer choose between diversity and peak-power reduction.

6.2 Extension of ACE to Rotated Constellations

After the forward mapping takes place, a square-like constellation is formed with non-uniformly-spaced constellation points. If QPSK signalling is originally used (i.e., as in Fig. 6.1), after rotating the constellation in the manner described above, a 16-QAM-like constellation is constructed as in Fig. 6.2. Similarly, if 16-QAM is used as the original constellation (i.e., as in Fig. 6.4), a 256-QAM-like constellation results as in Fig. 6.5. Therefore, one can perform SISO ACE, just as described in [12], by extending the outer constellation points of the expanded constellation in such a way that the peak power is reduced, just as shown in Figures 6.3 and 6.6.

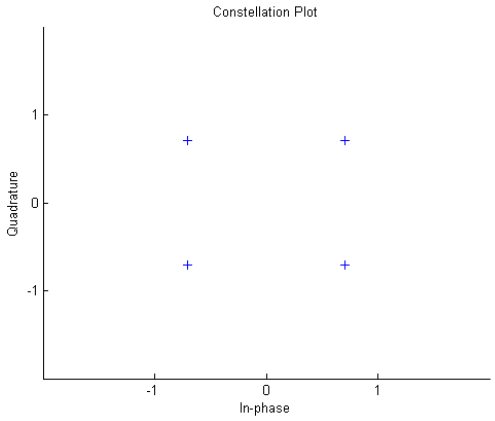

Figure 6.1: Original QPSK constellation.

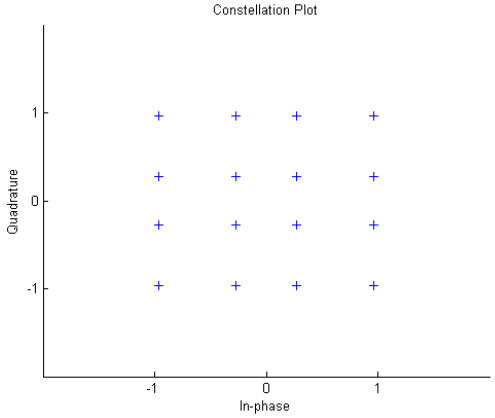

Figure 6.2: Extended QPSK rotated constellation with a rotation angle of 29°.

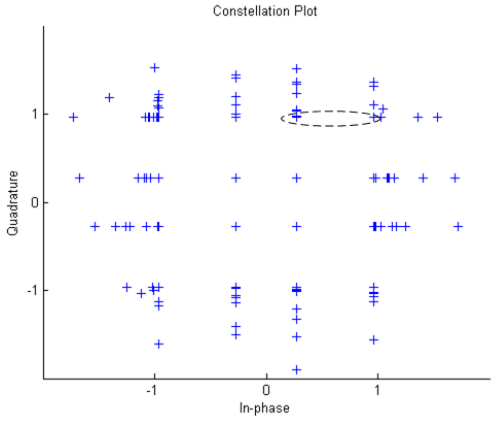

Figure 6.3: Extended QPSK rotated constellation with a rotation angle of 29° and ACE applied.

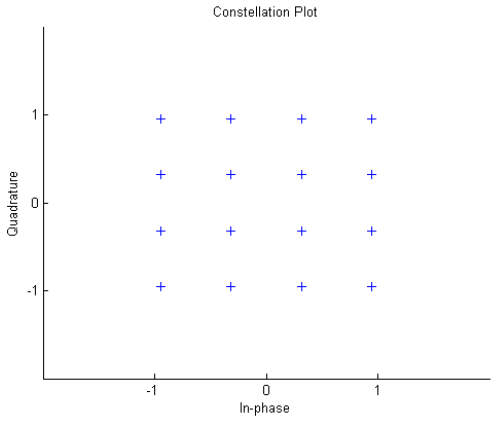

Figure 6.4: Original 16-QAM constellation.

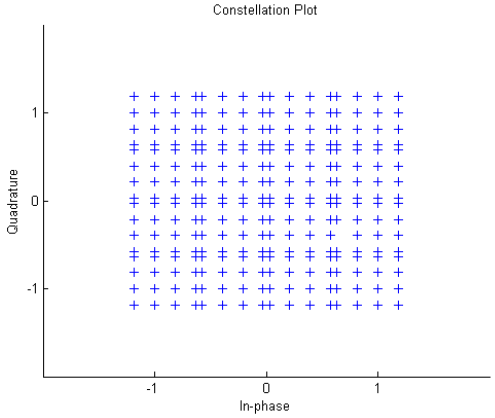

Figure 6.5: Extended 16-QAM rotated constellation with a rotation angle of 16.8°.

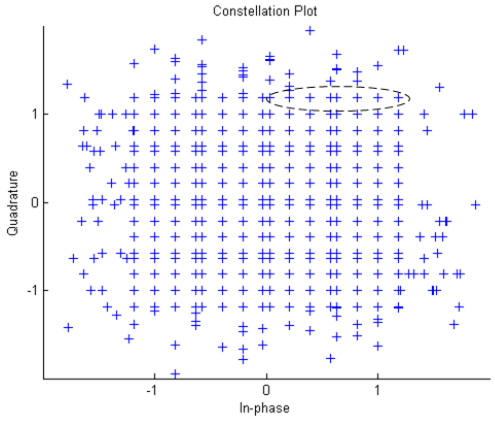

Figure 6.6: Extended 16-QAM rotated constellation with a rotation angle of 16.8° and ACE applied.

To do that, one needs to know the coordinates of the outer constellation points in order to appropriately perform the ACE projections (slice the outer regions non-uniformly to obtain the ACE projection regions) onto the set of allowable ACE vectors. Due to the symmetry of rotation (see Figures 6.1, 6.2, 6.4, 6.5), it suffices to compute only the real coordinates of half of the first quadrant rotated-and-cyclically-shifted outer constellation points, as highlighted in Fig. 6.3 and Fig. 6.6.

This can easily be done using the following formula. Let $X_k = a_k + jb_k$ denote the symbol loaded into the kth OFDM channel, and the I-Q pair (a_k, b_k) to be chosen from a QAM constellation C. Then, we have

$$\Re\{G_k\} = a_k \cos\left(\frac{2\pi\phi^\circ}{360}\right) - b_k \sin\left(\frac{2\pi\phi^\circ}{360}\right) \tag{6.3}$$

The coordinates of the rest of the outer constellation points can be easily found by symmetry.

At the receiver, in high signal-to-noise (SNR) scenarios, two steps may be taken to avoid bit-error-rate (BER) increase due to the induced ACE extensions. First, the extended constellation points are projected back to their rotated-and-cyclically-shifted constellation points and inverse mapping takes place to recover X_k. Second, inverse mapping can take place first to arrive at the original QPSK or 16-QAM constellation, then project the points back to the nearest original QPSK or 16-QAM point, and finally decode. On the other hand, in low SNR scenarios and severe fading (i.e., fading channels characterized by long delay-spreads), clustering will help, if only a little. Thus, it is important to consider different alternatives. A third alternative is to modify the log-likelihood ratios that are usually used to make hard or soft decisions on the coded bits. Inner and outer decoding follow to recover the information bits. A last alternative is to modify the demodulator and decoder unit and use a soft-input soft-output (SISO) unit [20] and then jointly demodulate and decode, in a manner similar to that described for tone injection for coded-OFDM systems in Chapter 7. The SISO unit may be initialized

with prior probabilities for each symbol in the rotated constellation, and some nonzero probability needs to also be assigned to the points lying on the ACE extended regions (i.e., through averaging statistics over a large number of OFDM blocks). The demodulator will need to be modified appropriately to handle the probability mapping from rotated constellation points to the regular QAM constellation points. Then, the regular sum-product (or min-sum) [21] inner LDPC decoder [2] may be initialized properly using the corresponding demodulator's output. We believe this last alternative is the most convenient and promising choice for the DVB-T2 standard, since OFDM is almost always used in conjunction with coding and this decoding scheme is compatible with the iterative demodulation-decoding flavor that turbo-coded systems usually exhibit [21].

Future work may involve examining the above-described decoding alternatives, in light of arriving at a net gain result on the achievable PAPR reduction, while keeping the possible BER increase below a certain level.

6.3 Simulation Results

Figures 6.3 and 6.6 show example runs of the extended constellations for the QPSK and 16-QAM original constellations, respectively. As shown, only the outer constellation points are moved, and since the clipping threshold, A, is not set too low, the outer rotated constellation points tend to remain clustered at their original locations. It is worthwhile to note that setting the clipping threshold unrealistically low leads to convergence problems, since outer constellation points tend to shoot outwards too far and subsequent iterations have difficulty lowering the PAPR. On the other hand, setting the clipping threshold too high may not unlock the full potential of ACE. Figures 6.3 and 6.6 show that the average transmit energy is slightly increased by 0.84 dB and 0.58 dB under QPSK and 16-QAM modulation respectively (for 256 subchannels), to lower the peak level of the transmit analog signal.

An example of the ACE-SGP algorithm results for SISO OFDM on rotated

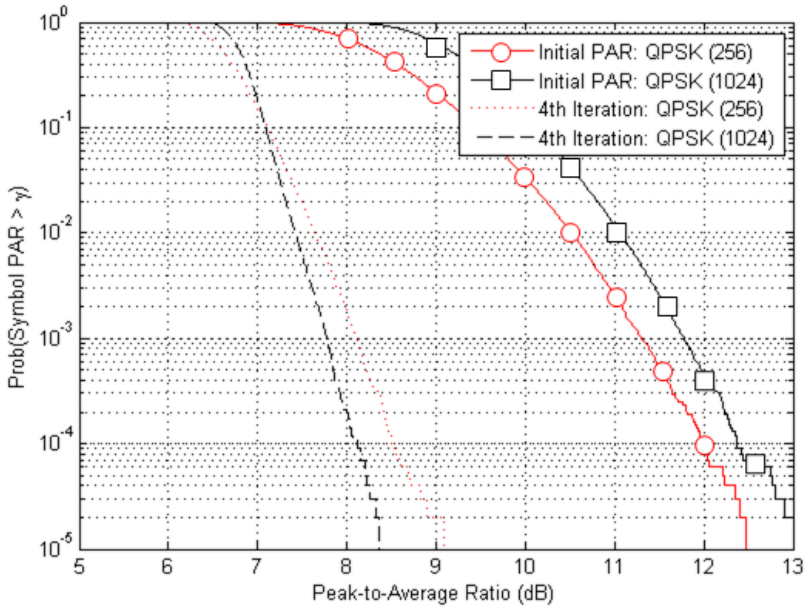

Figure 6.7: CCDF results using QPSK as the original constellation with 256 and 1024 subcarriers.

constellations is shown in Figure 6.7. The algorithm was tested for a complex-baseband OFDM signal with $N = 1024$ subchannels employing rotated-and-cyclically-shifted QPSK using 10^5 randomly generated OFDM symbol blocks. A level A of 7.5 dB above the average power was used to obtain the clipped signal to project onto the space of allowable extension vectors and an upsampling factor of $L = 8$ was used to approximate analog PAR reduction. Failure to process oversampled digital signals leads to large 'peak regrowth' at the A/D converter. Oversampling was performed by zero-padding in the frequency domain and using oversampled IFFT operations [12]. Figure 6.8 shows similar results for a complex-baseband OFDM signal with $N = 1024$ subchannels employing rotated-and-cyclically-shifted 16-QAM using 10^5 randomly generated OFDM symbol blocks. A level A of 8.0 dB above the average power was used to obtain the clipped signal to project onto the space of allowable extension vectors, and an upsampling factor of $L = 8$ was used to approximate analog PAPR reduction. The rotation angles were obtained according to [2] and four ACE-SGP iterations were used.

When QPSK is originally used, the reduction in PAPR obtained was 3.46 dB

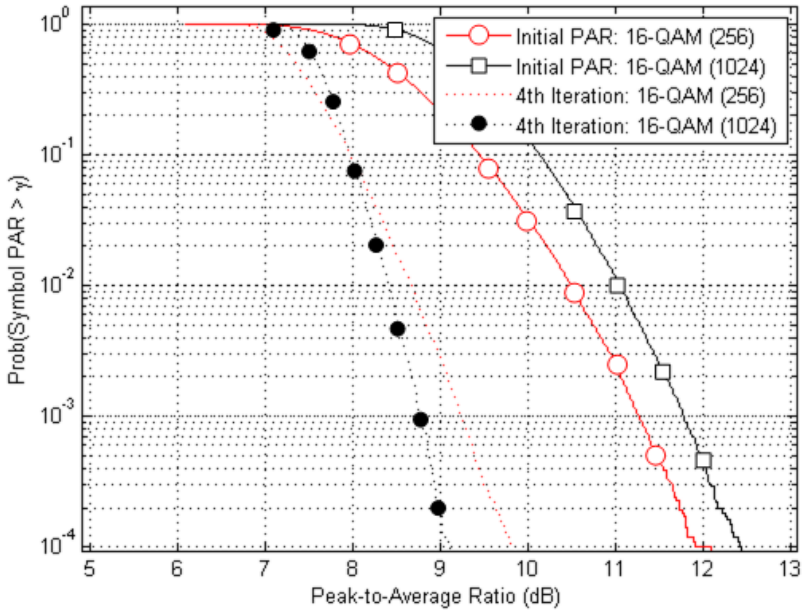

Figure 6.8: CCDF results using 16-QAM as the original constellation with 256 and 1024 subcarriers.

under 256 subcarriers and 4.29 dB under 1024 subcarriers when looking slightly above a 10^{-4} symbol clip probability level. Similarly, when 16-QAM is originally used, the reduction in PAPR obtained was 2.08 dB under 256 subcarriers and 3.41 dB under 1024 subcarriers. Just as described in [12], ACE PAPR reduction performance increases as the number of subcarriers increases. This further motivates the use of ACE as a peak-power reduction technique for the DVB-T2 standard since the FFT block size ranges from 1024 to 32768 subcarriers, depending on the reception conditions and operating area. ACE peak-power reduction can also be applied in the MISO mode that the DVB-T2 standard describes as an option for obtaining transmit diversity, where a variant of space-frequency block-coded Alamouti is used [2].

CHAPTER 7

PEAK-POWER REDUCTION FOR CODED OFDM SYSTEMS VIA TONE INJECTION

7.1 Tone Injection

Tuna's tone injection via agressive clipping projection algorithm (TI-ACP) [13] was tested for a complex-baseband OFDM signal using 10^6 randomly generated OFDM symbols. To approximate the analog PAPR, the transmit signal is oversampled by $L = 4$ prior to TI-ACP. Figure 7.1 (from [13]) shows the analog-approximated PAPR results of up to nine TI-ACP iterations for an $N = 128$ 16-QAM OFDM system. An approximated-analog PAPR reduction of 4.9 dB is achieved at a 10^{-5} clip probability after the ninth iteration, where the average power increase was 0.37 dB. This could be lowered if a higher target PAPR level was chosen. Tuna's tone injection thus provides unprecedented PAPR reduction that approaches the single-carrier PAPR of large (e.g., 64-QAM) constellations.

7.2 Coding for Tone Injection

OFDM provides frequency diversity by modulating many low-rate streams simultaneously and using error-correction capacity-achieving codes to spread the individual bits across a large bandwidth. The advantage is that if some particular range of frequencies are deeply faded, the overall signal can still be demodulated in a robust way. Thus, coding is critical in order to exploit OFDM as much as possible. However, most literature on PAPR has not looked at finding practical PAPR reduction algorithms for coded-OFDM systems. In other words, coding is treated as a separate entity and to avoid changing the state-of-the-art decoders,

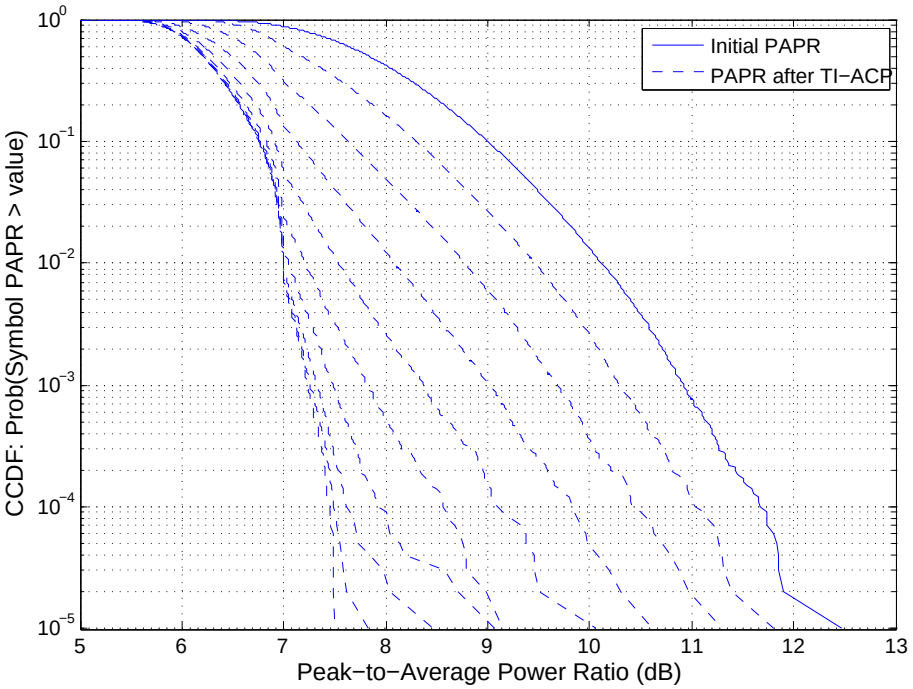

Figure 7.1: PAPR results of the TI-ACP method applied at $L = 4$ to an $N = 128$ 16-QAM OFDM system (from Tuna). The broken lines denote the CCDF obtained after each tone injection.

many PAPR reduction methods tend to sacrifice useful resources of wireless systems such as bandwidth, data rate, etc. (see Section 3.2). However, this raises the following question: Assuming a coded-OFDM system and alternative encoding at the transmitter (i.e., tone injection, rotated constellations, etc.) to lower the PAPR of the transmit signal, how do we optimally (or suboptimally) design the corresponding decoder to achieve the same bit-error rate (BER) performance of the link? In other words, with virtually no BER sacrifice, can we achieve the PAPR benefits that tone injection gives? The answer is yes.

When using tone injection, one of the worst-case scenarios is that we have a point slightly outside the main constellation. Let us assume for the moment that we have performed forward error-correction (FEC) using a convolutional encoder. If we perform the modulo-operation [4] (in Fig. 7.2, this corresponds to the mapping from symbol X to symbol X_{mod}) and then run the Viterbi decoder [22], decoding errors are very likely to occur because the distance measure has changed and has

not been accounted for.

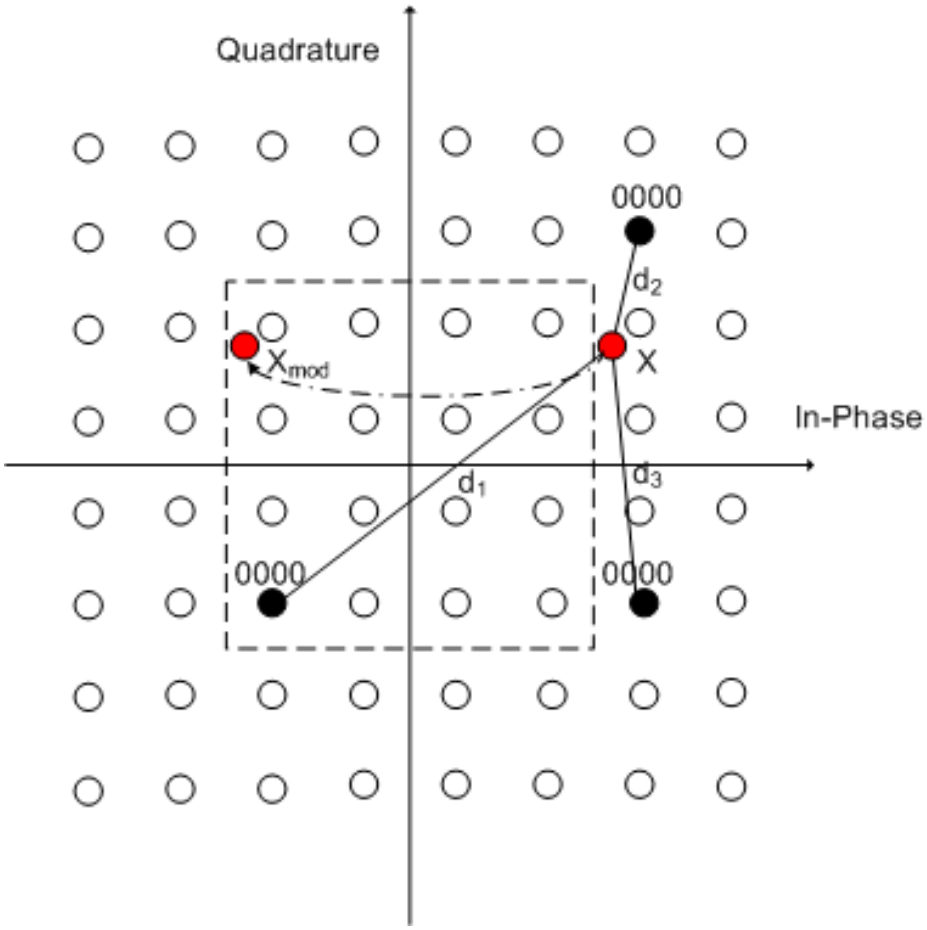

Figure 7.2: Simple example of tone injection for 16-QAM coded-OFDM. It is ambiguous how to optimally design a decoder that simultaneously demodulates and decodes data properly. In this case, let us assume that the symbol in black is associated with the bit sequence 0000.

From Fig. 7.2, it is clear that if no tone injection was used, the Euclidean distance metrics used for the Viterbi decoder would regard the probability of the red symbol (labeled as X) being the black one (inside the main constellation) as very small. When tone injection is used, we need to account for the cyclically extended constellation points as well. An intuitive way to extend the Viterbi algorithm to this example is to consider distances d_1, d_2 and d_3 simultaneously when computing the branch metrics on the decoder trellis. This way of changing the Euclidean distance metrics, which are used for finding the minimum path through the trellis by the Viterbi algorithm, showed an improvement over

performing the modulo operation [4] and decoding with the regular Viterbi decoder, but not as much of a BER improvement as using the soft-input soft-output demodulator and decoder approach described below. Moreover, we want to make the decoding technique as flexible as possible, allowing other types of codes (i.e., LDPC, turbo) to be used with tone-injection as well.

Thus, to obtain excellent decoding performance, we decide to account for all the constellation points using soft-input soft-output (SISO) demodulators and decoders. By using probability-based demodulators and decoders, we maintain the ability to perform iterative suboptimal demodulation and decoding (although the individual steps are optimally performed) jointly.

7.3 SISO Demodulator

The *soft-input soft-output* (SISO) demodulator computes the *a posteriori* probabilities of the coded bits given their *a priori* probabilities [20]. The k-bit information sequence is first encoded by a FEC encoder, constructing the n-bit codeword $\mathbf{c}$. Then, QAM modulation is performed; every set of q bits in codeword $\mathbf{c}$ gets mapped to one constellation point χ, which belongs to the main constellation C of size $M = 2^q$ (i.e., by the mapping β), constructing the transmitted discrete-time signal $\mathbf{x}$. Let the labeling function $\gamma(\chi_i, j) = b$ define the label for symbol χ_i having the jth bit equal to b. The received signal during the kth symbol period is

$$y_k = h_k x_k + n_k \tag{7.1}$$

where n_k denotes the zero-mean complex Gaussian noise random variable with variance σ^2 per dimension, y_k is the kth received symbol, and h_k is the complex channel gain representing the fading channel. For AWGN channels, $h_k = 1$.

The *a posteriori* coded bit probabilities can be calculated as

$$Pr(c_k^j = b|y_k) = \sum_{x_k \in C_b^j} Pr(x_k|y_k)$$
$$\propto \sum_{x_k \in C_b^j} Pr(y_k|x_k)Pr(x_k) \tag{7.2}$$

where $b \in \{0,1\}$, $C_b^j = \{\chi \in C : \gamma(\chi, i) = b\}$ and c_k^j denotes the jth bit of the kth symbol, x_k. For the tone-injection algorithm proposed here, the *a priori* symbol probabilities $Pr(x_k)$ were initialized based on Monte Carlo simulation results averaged over 100 OFDM blocks, for the first decoding iteration. After the first iteration, the *a priori* symbol probabilities need to be updated. Assuming a good bit interleaver was used, due to independence between the coded bits,

$$Pr(x_k) = \prod_{i=1}^{q} Pr(c_k^i = \gamma(x_k, i); I) \tag{7.3}$$

where $Pr(r; I)$ denotes the intrinsic information of the random variable r. We compute the extrinsic information (see [20]) for the second iteration as

$$Pr(c_k^j = b; O) = \frac{Pr(c_k^j = b|y_k)}{Pr(c_k^j = b; I)}$$
$$\propto \frac{\sum_{x_k \in C_b^j} Pr(y_k|x_k)Pr(x_k)}{Pr(c_k^j = b; I)} \tag{7.4}$$
$$= \sum_{x_k \in C_b^j} \left[Pr(y_k|x_k) \prod_{i \neq j} Pr(c_k^i = \gamma(x_k, i); I) \right] \tag{7.5}$$

where $Pr(y_k|x_k)$ depends on the channel model and noise statistics. After each iteration, the extrinsic bit probabilities are weighted such that $Pr(c_k^j = 0; O) + Pr(c_k^j = 1; O) = 1$ for all $\{k, j\}$. The decoding algorithms that follow require proper initialization of the *a posteriori* probabilities for the coded bits.

Note that due to Equations (7.2) and (7.4), to compute the *a posteriori* probability of the jth coded bit of the kth symbol, we need to sum over all symbols

in the extended constellation. This key step incorporates all the distances in the constellation domain in one metric, $Pr(c_k^j = b; O)$, which is then used by the decoders. Thus, the decoders only need the soft information for the coded bits provided by the demodulator.

7.4 SISO Convolutional Coding

Convolutional codes are popular error-correcting codes with encoders described by a finite-state machine (FSM). Encoding can be done via an encoding circuit constructed from generator polynomials. For a k/n-rate convolutional code, k information bits get mapped into n bits in a way that depends on the present k information bits and on previous information bits as well. The Viterbi algorithm has become the standard for decoding convolutional codes. More information on convolutional codes can be found in [22].

Convolutional decoding can also be performed via the forward-backward algorithm. In the literature, this also goes under the name of the BCJR (or MAP) algorithm [23] which was designed to compute the posterior probability of symbols generated from Markov sources sent through discrete memoryless channels. Using first principles from probability, the BCJR algorithm estimates the posterior probabilities for the message bits given the received data. Using the joint demodulation and high-radix decoding approach discussed in [24] would be far too expensive as the number of tone-injected points grows. A variant of the forward-backward algorithm operating on trellis edges was described in [20] and is used here as a soft-input soft-output convolutional decoder. The advantages of using this algorithm are that the trellis does not expand to account for the tone-injected constellation points, the *a posteriori* information for the coded bits provided by the demodulator can be easily incorporated into the convolutional decoder, and the algorithm is able to cope with a trellis with parallel edges.

The k/n-rate convolutional encoder maps a sequence of T input symbols $\{U_k\}_{k=1}^{T}$ (each chosen from alphabet $U := \{u_1, \ldots, u_{N_I}\}$), each characterized by k

bits into a sequence of output (code) symbols $\{C_k\}_{k=1}^{T}$ (each chosen from alphabet $C := \{c_1, \ldots, c_{N_O}\}$), each consisting of n bits. The *a priori* probability densities associated with each input and output symbol are given by $Pr(U_t; I) = \prod_{j=1}^{k} Pr(u_t^j; I)$ and $Pr(C_t; I) = \prod_{j=1}^{n} Pr(c_t^j; I)$, respectively. These forms of probability distributions are justified since bit interleavers are used. Note that $Pr(c_t^j; I)$ are provided by the demodulator.

The idea is that the dynamics of the time-invariant convolutional code are completely specified by one trellis section which describes the transitions (i.e., edges) between trellis states from time k to time $k+1$. One trellis section consists of a set of N states $S = \{s_1, \ldots, s_N\}$ and a set of $N \cdot N_I$ edges obtained by the Cartesian product $\mathbb{E} = S \times U = \{e_1, ..., e_{N \cdot N_I}\}$ which represent all possible transitions between states.

The starting state $s^S(e)$, ending state $s^E(e)$, input symbol $u(e)$ and output symbol $c(e)$ are the four parameters associated with each edge $e \in \mathbb{E}$. The starting state and input symbol uniquely identify the ending state because, given the initial trellis state, there is a bijective mapping between the input sequence and the state sequence.

The *a posteriori* probability distributions for the jth coded and information bit within are computed as follows for a k/n-rate time-invariant convolutional code:

$$Pr(c_t^j = b; O) \propto \sum_{e: C_t^j(e) = b} \left[\alpha_{t-1}(s^S(e)) Pr(U_t; I) Pr(C_t; I) \beta_t(s^E(e)) \right] \tag{7.6}$$

$$Pr(u_t^j = b; O) \propto \sum_{e: U_t^j(e) = b} \left[\alpha_{t-1}(s^S(e)) Pr(U_t; I) Pr(C_t; I) \beta_t(s^E(e)) \right] \tag{7.7}$$

where $b \in \{0, 1\}$ and the proportionality constants are chosen such that $Pr(c_t^j = 0; O) + Pr(c_t^j = 1; O) = 1$ and $Pr(u_t^j = 0; O) + Pr(u_t^j = 1; O) = 1$, $\forall t, j \in \{1, \ldots, q\}$.

The $\alpha_t(\cdot)$ and $\beta_t(\cdot)$ probabilities present in (7.6) and (7.7) are obtained

through the forward and backward recursions:

$$\alpha_t(s) = \sum_{e:s^E(e)=s} \left[\alpha_{t-1}(s^S(e))Pr(U_t(e);I)Pr(C_t(e);I)\right] \tag{7.8}$$

$$\beta_t(s) = \sum_{e:s^S(e)=s} \left[\beta_{t+1}(s^E(e))Pr(U_{t+1}(e);I)Pr(C_{t+1}(e);I)\right] \tag{7.9}$$

with initial values $\alpha_0(s) = 1$ if $s = S_0$ and $\alpha_0(s) = 0$ otherwise; $\beta_T(s) = 1$ if $s = S_T$ and $\beta_T(s) = 0$ otherwise. [3] Intuitively, the probabilities $\alpha_t(s)$ and $\beta_t(s)$ correspond to $Pr(C_1, \ldots, C_t, S_t = s)$ and $Pr(C_{t+1}, \ldots, C_T | S_t = s)$, respectively. So, to compute $\alpha_t(s)$, note that the transition to state s could have come from any state s' for which there is an edge joining state s' with s. Thus, it is required to sum up the probability of each edge (i.e., $Pr(U_t(e);I)Pr(C_t(e);I)$) times the previous $\alpha_{t-1}(s)$, over all edges that end up at state s. A similar intuitive interpretation can be provided for the recursive computation of $\beta_t(s)$.

As shown in (7.6), to compute $Pr(c_t^j = b; O)$, it is required to sum up the product of the probability of observing the output symbol sequence $\{C_1, \ldots, C_{t-1}\}$ and reaching state $s^S(e)$, the probability of going through edge e at time t (triggering edge $e \in \mathbb{E}$ through the input symbol $U_t(e)$ and observing $C_t(e)$) and the probability of observing $\{C_{t+1}, \ldots, C_T\}$ given that $s^E(e)$ is the ending state, over all edges that are associated with the jth bit of the tth output symbol being equal to b.

The implementation of this algorithm presented in the simulation results is a slightly modified version of this (based on the turbo principle), just as described in [20]. In short, the soft-input soft-output (SISO) APP unit [20], used here for convolutional decoding, can be thought of as a "device" that accepts the input distribution of the information bits and the input distribution of coded bits, and outputs the output distributions of the information and coded bits. The input distribution of the coded bits is provided by the demodulator (see (7.5)) and the

[3] Note that for tail-biting convolutional codes, S_0=S_T.

input distribution of the information bits is initialized to be uniform. The output distribution of the coded bits can be stored to be used in the next decoding iteration (optional) or discarded, and the output distribution of the information bits can be thresholded to make hard decisions on the information bit sequence.

7.5 SISO LDPC Coding

LDPC codes are sparse linear block codes characterized by a parity-check matrix, H. For an (N, k) linear block code, k information bits get mapped into N coded bits (where $N \geq k$), so the code rate is k/N. In this setup, H is of size $M \times N$, where $M = N - k$ is the number of parity checks and N is the block length. The matrix H defines the parity-check equations and can be represented as a bipartite graph. In short, $\mathbf{c}$ is a codeword if $H\mathbf{c} = \mathbf{0}$. More detailed information about LDPC codes can be found in [25] and [22].

The code considered here is an irregular Gallager code of rate 1/2. To construct the parity-check matrix (i.e., of size 256×512), H, with column-weight of 3, four steps were taken (see [26]). First, the required number of 1's were placed in each of the 512 columns randomly and the row-weight was kept as uniform as possible. Second, {1}'s were added to H to empty rows or rows that have only one 1 in them, randomly. Third, if the matrix constructed in the first step had an even number of 1's per column, we add up to two 1's at random positions. Finally, the number of length-4 cycles was reduced.

It is well known that LDPC codes can be efficiently decoded using message-passing on a Tanner graph, leading to the sum-product algorithm [27]. The *a posteriori* coded bit information provided by the demodulator was used as *a priori* information to initialize the sum-product decoder.

7.6 Simulation Results

Simulation results are shown in Figures 7.3 and 7.4 for tone-injection convolutionally-coded and LDPC-coded OFDM transmission and reception under the classic AWGN channel. The PAPR reduction obtained was 4.75 dB when looking at a 10^{-4} clip level and the average power increase is 0.19 dB. As shown in Figures 7.3 and 7.4, the performance gap is slightly less than 0.5 dB for both cases when looking at a BER of 10^{-3}.

To investigate the tone injection decoding performance in a more realistic wireless setting, we consider the case of a Rayleigh fading environment. Assuming a bandwidth of 20 MHz, an RMS delay spread of 50 ns and perfect channel state information (CSI) available at the receiver, we obtain the BER results shown in Figures 7.5 and 7.6. Testing the tone injection-decoding performance under Rician fading with a K-factor of 2, an RMS delay spread of 50 ns and perfect CSI available at the receiver, we obtain the BER results shown in Figures 7.7 and 7.8.

We maintain the benefit of PAPR reduction, while maintaining resistance to frequency-selective fading at a minimal BER increase and small average power increase. When testing under fading channels with a high degree of multipath, the BER difference is almost negligible. To sum up, we showed a practical way to obtain more than 4.5 dB overall PAPR reduction for the same BER, data rate and probability of clipping.

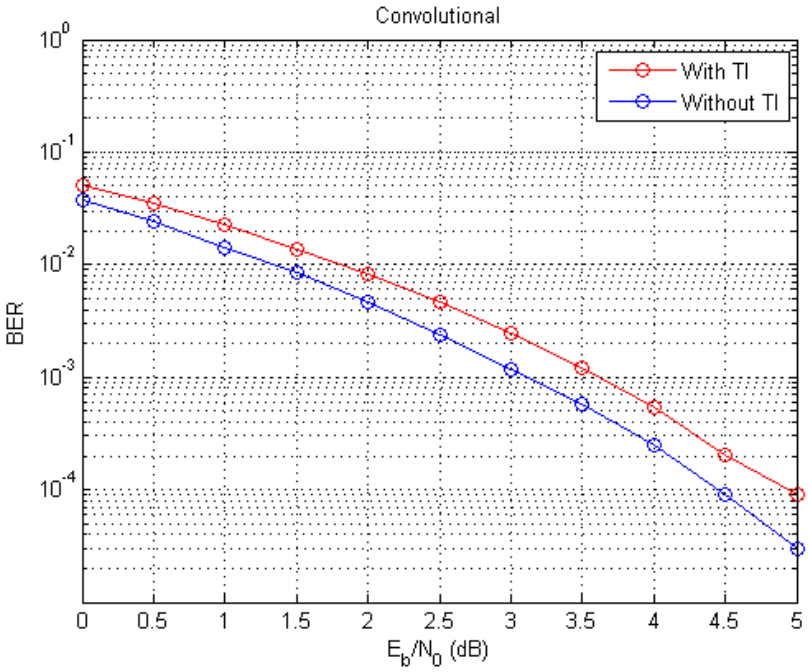

Figure 7.3: Tone-injection with 1/2 rate convolutional code under AWGN channel.

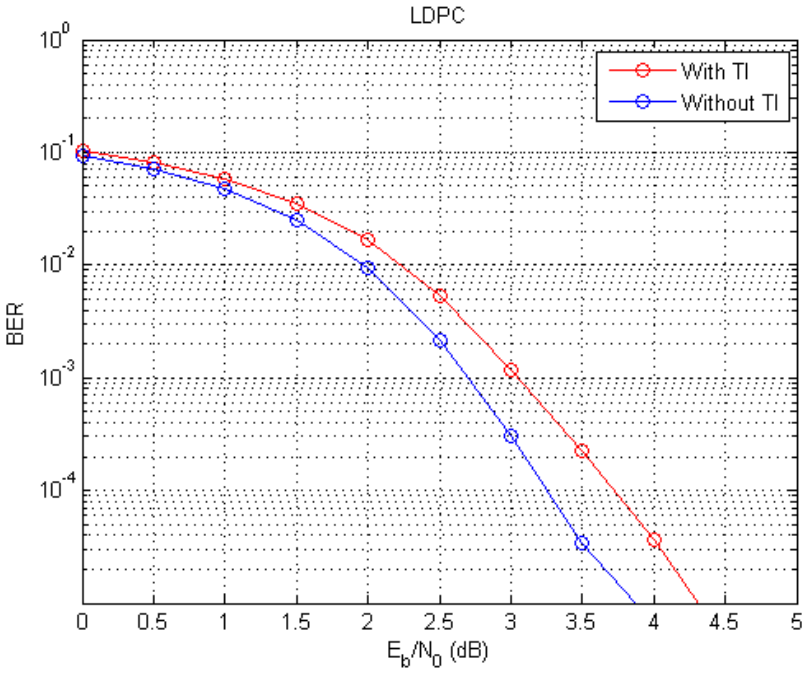

Figure 7.4: Tone-injection with 1/2 rate LDPC code under AWGN channel.

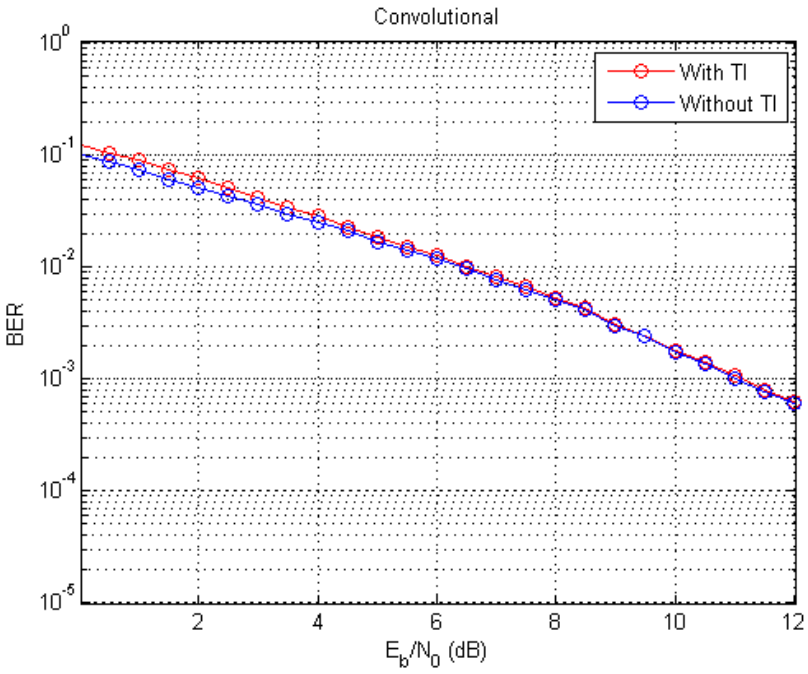

Figure 7.5: Tone-injection with 1/2 rate convolutional code under Rayleigh channel with RMS delay spread of 50 ns.

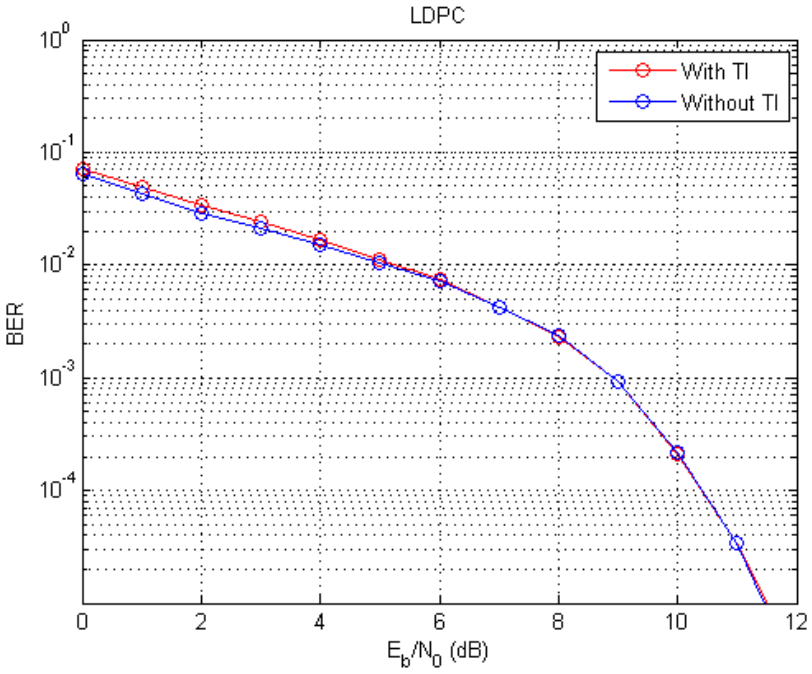

Figure 7.6: Tone-injection with 1/2 rate LDPC code under Rayleigh channel with RMS delay spread of 50 ns.

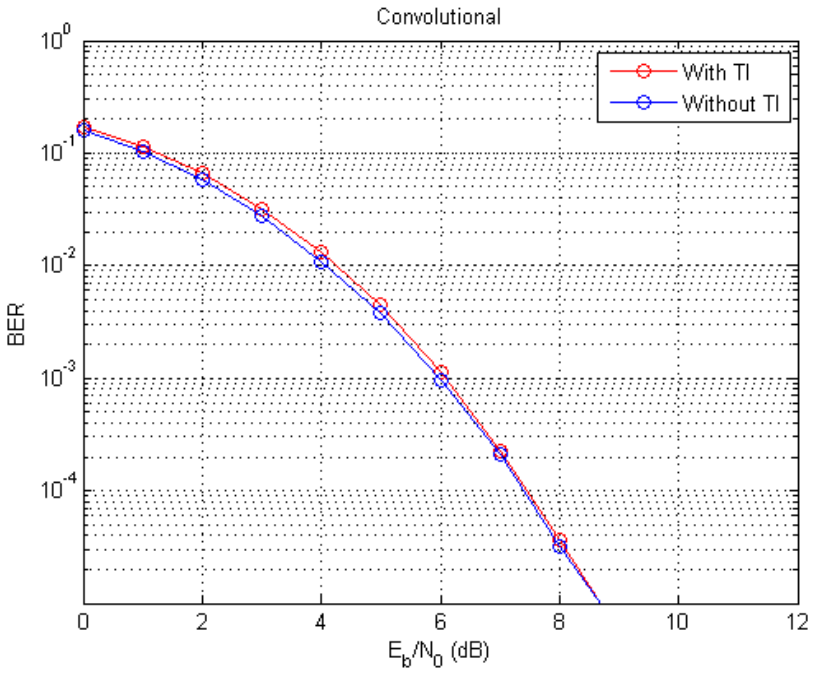

Figure 7.7: Tone-injection with 1/2 rate convolutional code under Rician channel with RMS delay spread of 50 ns and K-factor of 2.

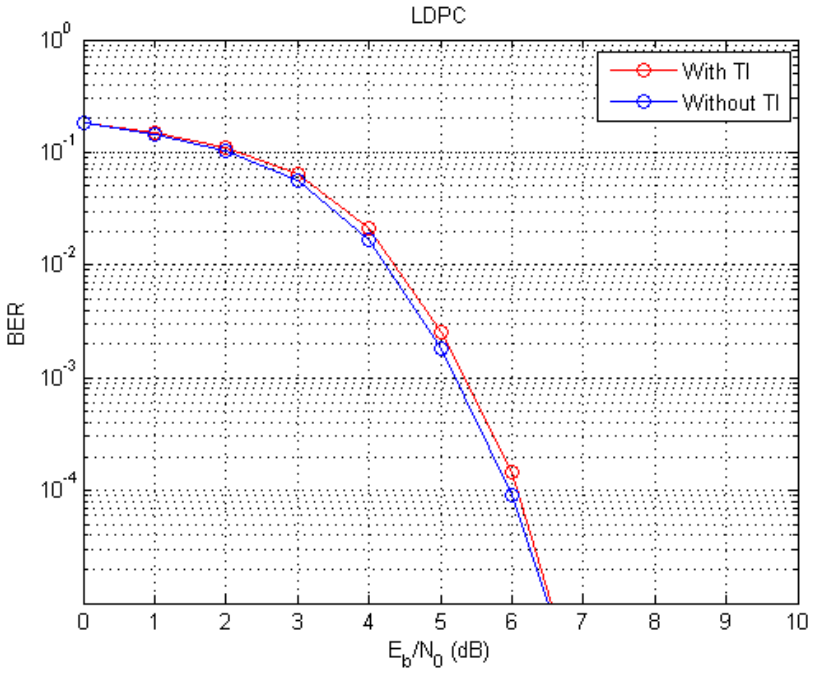

Figure 7.8: Tone-injection with 1/2 rate LDPC code under Rician channel with RMS delay spread of 50 ns and K-factor of 2.

CHAPTER 8

CONCLUSIONS

An extended method of ACE reduces the PAPR for space-time-frequency block coded MIMO-OFDM systems without compromising BER performance. Simulations showed that PAPR reduction gains of 4.19 and 3.57 dB can be obtained under QPSK for Alamouti STBC and SFBC, respectively. Gains above 4 dB were obtained for two and four antennas under QPSK for V-BLAST. Results show that as the number of antennas increases, the block code constraint reduces the ACE PAPR reduction gain for space-time/frequency-coded MIMO-OFDM systems, due to the reduced number of degrees of freedom caused by structured redundancy. On the other hand, the ACE PAPR reduction gain increases with the number of antennas for uncoded MIMO-OFDM systems (i.e., V-BLAST). The PAPR reduction gains obtained are larger than those observed for the SISO case [2].

The active constellation extension (ACE) method for PAPR reduction was extended to OFDM-based systems using rotated constellations. Simulation results show approximately 3.46 dB and 2.08 dB of PAPR reduction for QPSK and 16-QAM original constellations, respectively, under 256 subcarriers. Using the same clipping threshold, it was also shown that PAPR reductions of 4.29 dB and 3.41 dB are obtained under 1024 subcarriers for QPSK and 16-QAM, respectively.

The tone injection (TI-ACP) technique for PAPR reduction shows very promising results. Using the aggressive clipping approach [13], simulation results show approximately 4.9 dB of PAPR reduction at 10^{-3} symbol clip rate for 16-QAM constellations, with 128 subcarriers. To the best of our knowledge, tone injection was never considered as a practical peak-power reduction method, because all practical OFDM systems must use coding, and unless the appropriate decoders

are used, the BER performance will be severely degraded. We show how to design flexible decoders for coded-OFDM systems employing tone injection, making tone injection practical for the first time. Results showed that combining the fast TI-ACP method with coding yields excellent results both for convolutional and LDPC coded-OFDM systems. The technique can be extended to other codes as well (i.e., turbo, hybrid codes, etc.). Tuna's work [13] has shown that for 64-QAM constellations, the TI-ACP algorithm can closely approach the 64-QAM single-carrier PAPR performance. Putting this together with the coding techniques developed in this thesis, the PAPR problem is essentially solved for large constellations.

In light of obtaining larger PAPR gains, further work may include combinations of ACE and tone injection for SISO and MIMO-OFDM systems, as well as extensions to multiuser scenarios.

REFERENCES

[1] D. L. Jones, "Peak power reduction in OFDM and DMT via active constellation extension," in *Proceedings of the Asilomar Conference on Signals, Systems, and Computers*, vol. 2, 1999, pp. 1076–1079.

[2] R. M. Neal, "Frame structure channel coding and modulation for a second generation digital terrestrial television broadcasting system (DVB-T2)," 2008, DVB Project. [Online]. Available: http://www.dvb.org/technology/standards/a122.tm3980r5.DVB-T2.pdf

[3] J. Stott, "DTG DVB-T2 implementers' seminar: Rotated constellations," 2008. [Online]. Available: http://www.dtg.org.uk/dtg/t2docs/RotCon_Jonathon_Stott_BBC.pdf

[4] J. Tellado, "Peak to average power reduction for multicarrier modulation," Ph.D. dissertation, Stanford University, Palo Alto, CA, 2000.

[5] D. Tse and P. Viswanath, *Fundamentals of Wireless Communication*. New York, NY: Cambridge University Press, 2005.

[6] S. Litsyn, *Peak Power Control in Multicarrier Communications*. New York, NY: Cambridge University Press, 2007.

[7] X. Li and C. J. Simini, "Effects of clipping and filtering on the performance of OFDM," *IEEE Communication Letters*, vol. 2, pp. 131–133, May 1998.

[8] B. S. Krongold and D. L. Jones, "A new tone reservation method for complex-baseband PAR reduction in OFDM systems," in *Proceedings of IEEE International Conference on Acoustics, Speech, and Signal Processing (ICASSP)*, Orlando, FL, May 2002, pp. 2321–2324.

[9] B. S. Krongold and D. L. Jones, "An active-set approach for OFDM PAR reduction via tone reservation," *IEEE Transactions on Signal Processing*, vol. 52, pp. 495–509, February 2004.

[10] A. Ghassemi and T. A. Gulliver, "A low-complexity PTS-based radix FFT method for PAPR reduction in OFDM systems," *IEEE Transactions on Signal Processing*, vol. 56, pp. 1161–1166, March 2008.

[11] R. Bauml, R. F. H. Fischer, and J. B. Huber, "Reducing the peak-to-average power ratio of multicarrier modulation by selected mapping," *IEE Electronic Letters*, vol. 32, pp. 2056–2057, October 1996.

[12] B. S. Krongold and D. L. Jones, "PAR reduction in OFDM via active constellation extension," *IEEE Transactions on Broadcasting*, vol. 49, pp. 258–268, September 2003.

[13] C. Tuna, "Tone injection with agressive clipping projection for wireless OFDM PAR reduction," M.S. thesis, University of Illinois at Urbana-Champaign, Urbana, IL, 2009.

[14] S. M. Alamouti, "A simple transmit diversity technique for wireless communications," *IEEE Journal on Selected Areas in Communications*, vol. 16, pp. 1451–1458, October 1998.

[15] V. Tarokh, H. Jafarkhani, and A. R. Calderbank, "Space-time block codes from orthogonal designs," *IEEE Transactions on Information Theory*, vol. 45, pp. 1456–1467, July 1999.

[16] A. V. Geramita and J. Seberry, *Orthogonal Designs, Quadratic Forms and Hadamard Matrices*. New York, NY: Marcel Dekker, 1979, vol. 45.

[17] E. G. Larsson and P. Stoica, *Space-Time Block Coding for Wireless Communications*. Cambridge, United Kingdom: Cambridge University Press, 2003.

[18] V. Tarokh, H. Jafarkhani, and A. R. Calderbank, "Space-time block coding for wireless communications: Performance results," *IEEE Journal on Selected Areas in Communications*, vol. 17, pp. 451–460, March 1999.

[19] P. Wolniansky, G. Foschini, G. Golden, and R. Valenzuela, "V-BLAST: An architecture for realizing very high data rates over the rich-scattering wireless channel," in *URSI International Symposium on Signals, Systems, and Electronics*, October 1998, pp. 295–300.

[20] S. Benedetto, D. Divsalar, G. Montorsi, and F. Pollara, "A soft-input soft-output APP module for iterative decoding of concatenated codes," *IEEE Communications Letters*, vol. 1, pp. 22–24, January 1997.

[21] T. K. Moon, *Error Correction Coding: Mathematical Methods and Algorithms*. Hoboken, NJ: Wiley, 2005.

[22] B. Sklar, *Digital Communications: Fundamentals and Applications*, 2nd ed. Upper Saddle River, NJ: Prentice Hall, 2001.

[23] L. R. Bahl, J. Cocke, F. Jelinek, and J. Raviv, "Optimal decoding of linear codes for minimizing symbol error rate," *IEEE Transactions on Information Theory*, vol. 20, pp. 284–287, March 1974.

[24] D. Gkrimpas and V. Paliouras, "On the complexity of joint demodulation and convolutional decoding," in *IEEE Workshop on Signal Processing Systems*, Shanghai, China, October 2007, pp. 669–674.

[25] R. G. Gallager, *Low-Density Parity-Check Codes*. Cambridge, MA: MIT Press, 1963.

[26] R. M. Neal, "Creating a parity-check matrix," 2001, Dept. of Statistics and Dept. of Computer Science, University of Toronto. [Online]. Available: http://www.cs.toronto.edu/ radford/ftp/LDPC-2001-05-04/pchk.html

[27] F. R. Kschischang, B. J. Frey, and H. Loeliger, "Factor graphs and the sum-product algorithm," *IEEE Transactions on Information Theory*, vol. 47, pp. 498–519, February 2001.